minerals

MDPI

Article

Trace Element Distribution in Magnetite Separates of Varying Origin: Genetic and Exploration Significance

Demetrios G. Eliopoulos [1] and Maria Economou-Eliopoulos [2,*]

[1] Institute of Geology and Mineral Exploration (IGME), Sp. Loui 1, Olympic Village, GR-13677 Acharnai, Greece; eliopoulos@igme.gr
[2] Department of Geology and Geoenvironment, University of Athens, 15784 Athens, Greece
* Correspondence: econom@geol.uoa.gr

Received: 10 November 2019; Accepted: 2 December 2019; Published: 6 December 2019

Abstract: Magnetite is a widespread mineral, as disseminated or massive ore. Representative magnetite samples separated from various geotectonic settings and rock-types, such as calc-alkaline and ophiolitic rocks, porphyry-Cu deposit, skarn-type, ultramafic lavas, black coastal sands, and metamorphosed Fe–Ni-laterites deposits, were investigated using SEM/EDS and ICP-MS analysis. The aim of this study was to establish potential relationships between composition, physico/chemical conditions, magnetite origin, and exploration for ore deposits. Trace elements, hosted either in the magnetite structure or as inclusions and co-existing mineral, revealed differences between magnetite separates of magmatic and hydrothermal origin, and hydrothermal magnetite separates associated with calc-alkaline rocks and ophiolites. First data on magnetite separates from coastal sands of Kos Island indicate elevated rare earth elements (REEs), Ti, and V contents, linked probably back to an andesitic volcanic source, while magnetite separated from metamorphosed small Fe–Ni-laterites occurrences is REE-depleted compared to large laterite deposits. Although porphyry-Cu deposits have a common origin in a supra-subduction environment, platinum-group elements (PGEs) have not been found in many porphyry-Cu deposits. The trace element content and the presence of abundant magnetite separates provide valuable evidence for discrimination between porphyry-Cu–Au–Pd–Pt and those lacking precious metals. Thus, despite the potential re-distribution of trace elements, including REE and PGE in magnetite-bearing deposits, they may provide valuable evidence for their origin and exploration.

Keywords: magnetite separates; trace elements; exploration; ophiolites; skarn; porphyry-Cu; Fe–Ni-laterites

1. Introduction

Magnetite is a widespread mineral, as disseminated or massive ore, in various geotectonic settings and rock-types, such as magmatic, hydrothermal, ophiolites, calk-alkaline rocks (porphyry-Cu deposits, skarn type), laterites, and metamorphosed rocks/ores, all formed under a variety of conditions [1–13]. It has an inverse cubic (space group *Fd3m*) spinel-type structure with the general stoichiometry AB_2O_4, where A and B are tetrahedral (Fe^{3+}) and octahedral (Fe^{3+} and Fe^{2+}) coordination sites, respectively [14]. In addition, the geochemistry of magnetite separates is also affected by the co-precipitation of other minerals [5–9]. Trace elements hosted either in the structure of magnetite, such as cations which can substitute on the A (Mg, Fe^{2+}, Ni, Mn, Co, or Zn) and B (Al, Cr, Fe^{3+}, V, Mn or Ga) sites [14,15], and/or in mineral inclusions. They may result in distinctive trace element signatures in magnetite separates and can be used as a prospective tool for many types of ore deposits, and/or a variety of trace-element discrimination diagrams can classify magnetite separates from different types of ore deposits [4–13]. However, it has been proposed that the discrimination diagram (Ti + V) versus (Ca + Al + Mn) can be

used with caution as a petrogenetic indicator for trace element data in the case of magnetite separates which have unusual composition and/or have been re-equilibrated. [16].

The present study is focused on massive and disseminated magnetite separates from various geotectonic settings covering a wide range of formation conditions: Hydrothermal magnetite associated with calc-alkaline rocks (skarn type, porphyry-Cu–Au deposit), ophiolite complexes (associated with sulphides or apatite), magmatic magnetite from the magmatic sequence of ophiolites and ultramafic lavas/wherlites, magnetite from metamorphosed laterites, and magnetite separates from black coastal sand. Major and minor/trace element contents, including rare earth elements (REEs), in these magnetite separate types are presented and are compared to literature data. The purpose of this application of the magnetite chemistry and texture features is to provide a potential relationship between compositional variation and physico/chemical conditions, the magnetite origin, and exploration of ore deposits.

2. Materials and Methods

2.1. Mineral Chemistry

Polished sections (two-tree samples from each type) from magnetite ores (Tables 1–4) were carbon- or gold-coated and examined by a scanning electron microscope (SEM) using energy-dispersive spectroscopy (EDS). The SEM images and EDS analyses were carried out at the University of Athens (NKUA), using a JEOL JSM 5600 scanning electron microscope (Tokyo, Japan), equipped with the ISIS 300 OXFORD automated energy dispersive analysis system (Oxfordshire, UK) with the following operating conditions: Accelerating voltage 20 kV, beam current 0.5 nA, time of measurement (dead time) 50 s, and beam diameter 1–2 μm. The following X-ray lines were used: FeKα, NiKα, CoKα, CuKα, CrKα, AlKα, TiKα, CaKα, SiKα, MnKα, and MgKα. Standards used were pure metals for the elements Cr, Mn, Ni, Co, Zn, V, and Ti, and Si, MgO for Mg, and Al_2O_3 for Al. Contents of Fe_2O_3 and FeO for spinels were calculated on the basis of the spinel stoichiometry. The H_2O for (Co, Mn, Ni)-hydroxides was calculated to obtain 2 (OH) *pfu*.

Whole Rock Analysis

The studied magnetite samples were massive and disseminated mineralizations, derived from large (weighing approximately 2 kg) samples, which were crushed and pulverized in an agate mortar. The samples of magnetite separates from the Skouries deposit are representative of increasing depth from 43 to 363 m (the depth for the sample skou8b was 280 m) [4]. The multi-stage water flotation was applied and magnetite separates were concentrated magnetically from the water suspension of the rock powder. This portion was furthermore pulverized in the agate mortar at a size fraction −75 μm, and magnetite separates were separated furthermore from silicates. Thus the magnetite separate concentrates with weak silicates and potential very fine inclusions of various minerals (SEM/EDS images; Table 1) were used for bulk rock analysis.

Major and minor/trace elements in magnetite separate samples and two samples from the extinct fumaroles co-existing with native sulphur from the volcanic environment in the Aegean Sea (Santorini and Nisyros islands) were determined at the SGS Global—Minerals Division Geochemistry Services Analytical Laboratories Ltd., Vancouver, BC, Canada. The samples were dissolved using sodium peroxide fusion, combined ICP-AES and ICP-MS (Package GE_ICP91A50). Detection limits of the method are provided (Table S1). On the basis of the quality control report provided by Analytical Labs, the results of the reference material analysis in comparison to expected values, and the results from multistage analysis of certain samples, showed accuracy and precision of the method in good agreement with international standard (<10%).

3. Geological Outline and Mineralogical Features

3.1. Hydrothermal Magnetite Separates

3.1.1. Massive Magnetite Separates of Skarn-Type (Lavrion, Plaka Mine)

The ancient (earlier than 1000 B.C.), famous mine of Lavrion in Attica (Greece) is associated with a granodiorite intrusion, of Upper Miocene age, within the metamorphic -Cycladic Crystalline belt, which belongs to the carbonate replacement deposits (CRDs) [17]. It is well known for the exploitation of mixed massive sulphide mineralization composed by sphalerite, pyrite and galena (B.P.G), especially the production of silver [17–20]. Early hornfels formation was followed by the multistage development of a skarn deposit at the area of Plaka, around the granodiorite body, located into two stratigraphic horizons, near the contacts between the Kaessariani schist with lower and upper marble (Figure 1) [2].

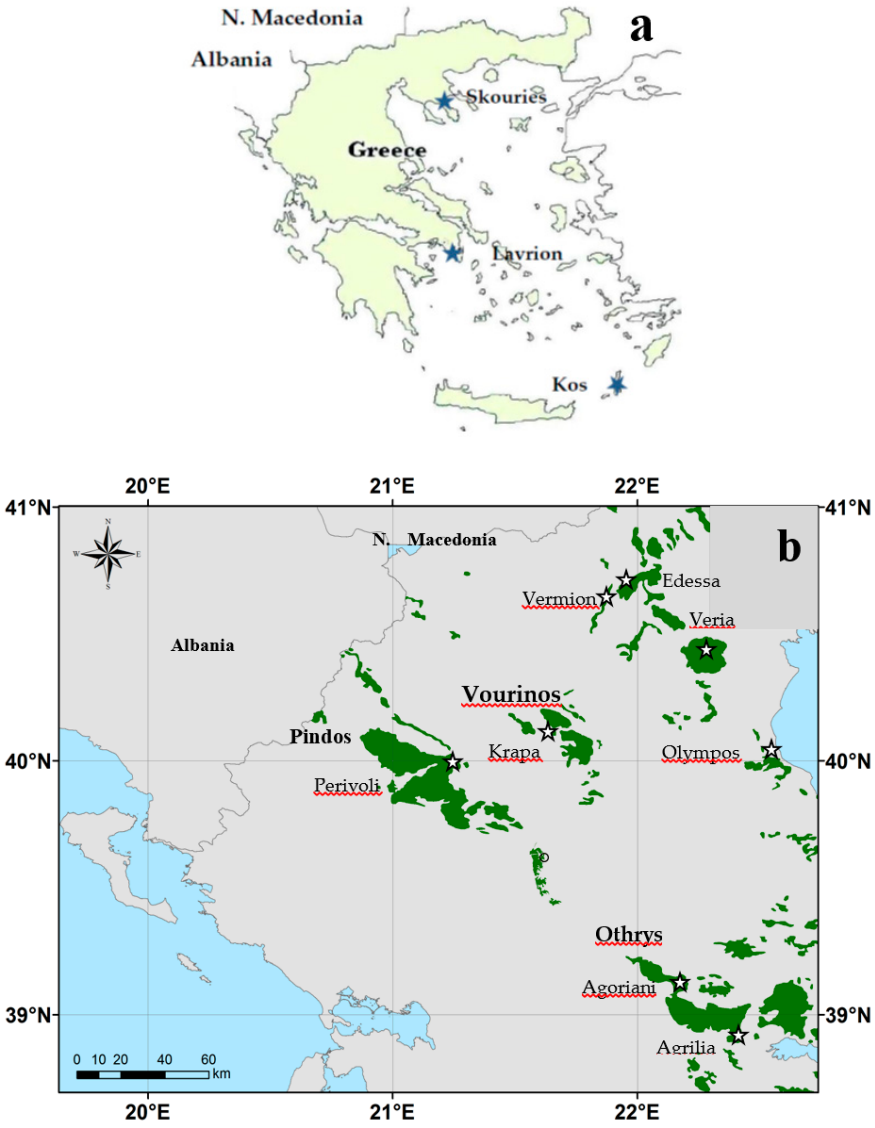

Figure 1. Sketch map showing the location of the studied magnetite separates hosted in calc-alkaline rocks (**a**). Ophiolitic rocks and metamorphosed Ni-laterite deposits (**b**).

Texture characteristics of the magnetite mineralization show multiple stages of the mineralization and that early magnetite and magnetite–hematite representing endoskarns (stage I) was followed by pyrite, pyrrhotite, and Fe-rich sphalerite, Ag-rich galena, arsenopyrite, forming exoskarns (stage II) [2,16] high-Fe sphalerite, chalcopyrite, and galena forming (Figure 2) [17–19]. Magnetite occurs as

euhedral or anhedral crystals, homogeneous or having abundant porosity and solid inclusions, mostly silicate minerals. It is almost pure, having very low Si, Al, and Mn contents, while Ti and V are lower than the detection limit (Table 1).

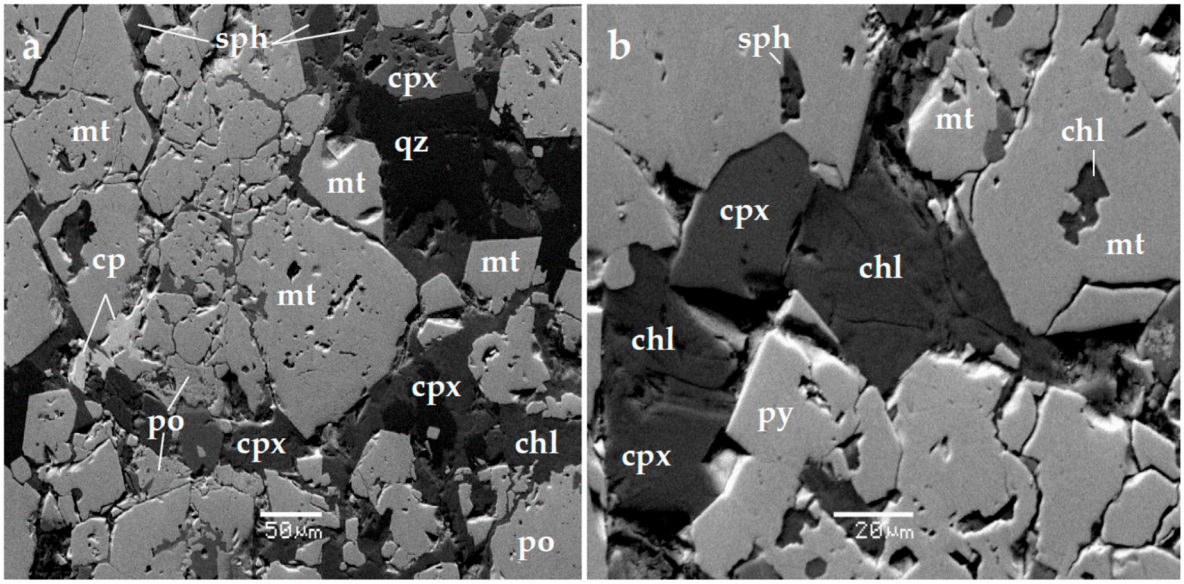

Figure 2. Back-scattered electron (BSE) images showing homogeneous magnetite separates (mt) in sharp contact with magnetite, having abundant porosity and solid inclusions, mostly silicate minerals, associated with clinopyroxene, quartz, chlorite, pyrrhotite, chalcopyrite, and sphlerite (**a**); magnetite is associated with silicates, sphalerite, and pyrite (**b**). Abbreviations: mt = magnetite; po = pyrrhotite; cp = chalcopyrite; py = pyrite; sph = sphalerite; cpx = clinopyroxene; qtz = quartz; chl = chlorite.

3.1.2. Disseminated Magnetite in Porphyry-Cu Deposit (Skouries)

The Skouries porphyry-Cu deposit is related to tertiary subvolcanic–porphyritic stocks, which belong to the Vertiskos Formation of the Serbo-Macedonian massif (SMM), Greece, and are controlled by deep fracture systems [21]. The typical alteration types of the porphyry-Cu intrusions are more or less presented in the Skouries intrusion, due to the repeated overprinting and intense silicification, with potassic being the predominant alteration type. Two mineral assemblages occurring as veinlets and disseminations can be distinguished: (1) Magnetite, reaching up to 10 vol.% (average 6 vol.%)—bornite–chalcopyrite, linked to pervasive potassic and propylitic alteration type, in the central parts of the deposit; and (2) chalcopyrite–pyrite, dominant at the peripheral parts of the deposit [4]. Chalcopyrite, and to a lesser extent bornite, contain occasional exsolutions of clausthalite (PbSe) (Figure 3b). There is a frequent association of magnetite separates and Cu-minerals (bornite and chalcopyrite) with inclusions of thorite, U-bearing thorite, rare earth element (REE)-enriched silicates of the epidote-group (allanite), Ce- and Th-rich monazites, and zircons identified as accessory minerals (Figure 3b–d; Table 1).

Table 1. Representative electron SEM/EDS analyses of magnetite in various rock-types (Figures 2–5, 7 and 8). Symbol n.d. = no detected.

	CALC-ALKALINE					**OPHIOLITES**							**PLACER**
Deposit type	Skarn-type			Hydrothermal		Hydrothermal				Magmatic			
Location	Lavrion			Skouries		Othrys	Edessa	Pindos	Vourinos	Vourinos	Othrys	Othrys	KOS
sample	Plaka P.L.mt1	Plaka P.L.mt2	SK43	SG-6	Skou8	Agoriani O.Ag.t	Samari EdK2	Perivoli Pi.Mt	Krapa VKMt	Krapa VKMt1	Agrilia 15Agr2	Agrilia O.Agr34	KOS1
wt.%													
SiO_2	1.7	2.6	0.9	0.7	0.4	0.5	2.3	0.3	0.5	0.9	0.3	0.7	0.5
Al_2O_3	0.5	0.9	n.d	n.d.	n.d.	0.6	0.2	n.d.	1.7	2.1	11.1	7.5	1.5
Cr_2O_3	n.d.	n.d.	2.1	0.9	n.d.	n.d.	0.1	n.d.	n.d.	n.d.	3.9	1.5	0.2
V_2O_5	n.d.	n.d.	0.7	0.5	n.d.	n.d.	n.d.	n.d.	1.4	1.8	0.7	0.6	0.5
Fe_2O_3	67.5	67.7	66.7	67.6	67.9	68.1	68.1	69.7	55.1	55.4	45.2	51.4	57.1
FeO	30.4	30.4	30.6	30.8	30.7	30.1	29.9	30.2	33.5	33.3	32.3	31.1	34.5
MgO	n.d.	0.3	n.d.	n.d.	0.5	0.9	n.d.	0.2	n.d.	0.9	3.1	3.5	n.d.
MnO	0.5	0.3	n.d.	n.d.	n.d.	n.d.	0.2	0.2	0.5	0.6	0.2	0.4	1.2
CoO	n.d.	n.d.	n.d.	n.d.	n.d.	n.d.	n.d.	n.d.	n.d.	n.d.	0.2	n.d.	n.d.
TiO_2	n.d.	n.d.	n.d.	n.d.	0.6	n.d.	n.d.	n.d.	6.9	4.4	3.6	4.6	5.1
Total	100.6	101.5	101	99.6	99.8	99.3	100.8	100.6	99.6	99.4	100.9	100.7	100.6

Table 2. Representative electron SEM/EDS analyses of fine-grained minerals associated with magnetite (Figure 3) from the Skouries porphyry-Cu deposit. Symbol n.d. = no detected.

wt.%	Monazite	Thorite	U-Thorite	Na, Ce-epidote	Allanite	Allanite
SiO_2	1.1	18.8	15.7	38.3	32.1	35.4
Al_2O_3	n.d.	n.d.	n.d.	27.2	16.2	14.1
FeO	n.d.	n.d.	0.6	8.3	14.9	17.4
CaO	0.8	n.d.	n.d.	22.2	12.4	13.6
P_2O_5	30.3	n.d.	n.d.	n.d.	n.d.	n.d.
ZrO_2	n.d.	n.d.	n.d.	n.d.	n.d.	n.d.
La_2O_3	17.2	n.d.	n.d.	0.9	5.1	3.9
Ce_2O_3	31.6	n.d.	n.d.	2.2	14.5	12.5
Nd_2O_3	10.5	n.d.	n.d.	n.d.	4.7	2.2
Pr_2O_3	2.8	n.d.	n.d.	n.d.	n.d.	n.d.
ThO_2	5.1	79.4	70.8	n.d.	n.d.	n.d.
UO_3	n.d.	n.d.	11.7	n.d.	n.d.	n.d.
Total	99.4	98.2	98.1	99.1	99.9	99.1

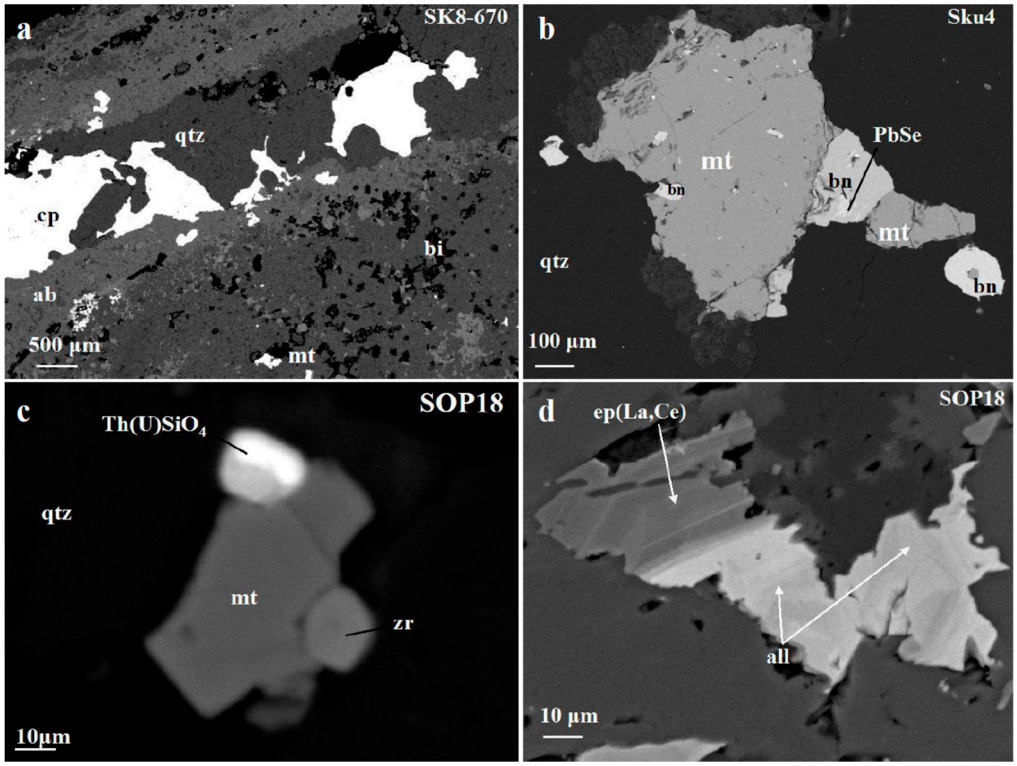

Figure 3. Back-scattered electron (BSE) images from the Skouries porphyry deposit, showing textural relationships between co-existing minerals. Quartz–chalcopyrite vein crosscutting biotite and magnetite-rich potassic altered porphyry (**a**); a close intergrowth of disseminated Ti–magnetite, chalcopyrite, bornite, and clausthalite (PbSe) (**b**); magnetite associated with thorite and zircon hosted by quartz (**c**); rare earth element (REE)-enriched epidote overgrown by allanite (**d**). Their composition is given (Table 2). Abbreviations: qtz = quartz; ab = albite; bi = biotite; mt = magnetite; cp = chalcopyrite; bn = bornite; PbSe = clausthalite; zr = zircon; ep = epidote; all = allanite.

3.1.3. Massive Magnetite Associated with Fe–Cu–Ni–Co Sulphides in Ophiolites (Pindos)

Sulfide mineralization in the Pindos ophiolite complex is located in the Smolicas Mountains, near the Aspropotamos dismembered ophiolite unit. This sequence, belonging to the ophiolitic unit of the Pindos complex, includes: (1) An intrusive section composed of dunites, lherzolites, olivine-websterites, olivine-gabbros, anorthosite gabbros, gabbros, and occasionally gabbronorites; and (2) a volcanic and

subvolcanic sequence composed mainly by basalts and basaltic andesite pillow lavas ranging from high- to low-Ti affinity [22,23]. At the Perivoli (Tsoumes Hill) of the Aspropotamos unit, within gabbro close to its tectonic contact with serpentinized harzburgite, small irregular to lens-like occurrences (4 m × 1.5 m) of massive sulfide mineralization of Fe–Cu–Ni–Co type have been described [24]. Magnetite, forming often a network texture, is associated with sulphides, either as massive ore with inclusions of sulfides (chalcopyrite, pyrite, and pyrrhotite), or as individual grains dispersed within sulfide ore. A salient feature of magnetite is a network texture with occasionally deformed crystals (Figure 4). The composition of magnetite separates is characterized by very low Al, Ti, Cr, Mn, Ni, and V contents (Table 1 and Table S1).

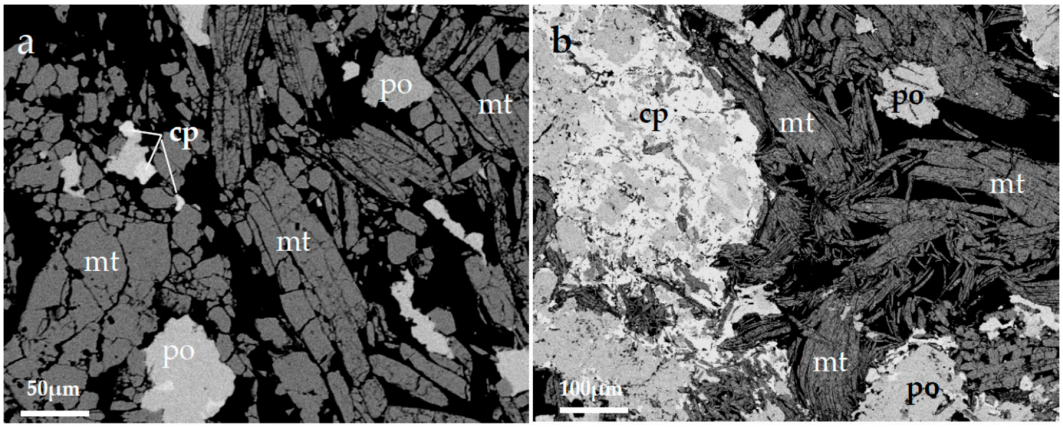

Figure 4. Back-scattered electron (BSE) images showing elongated curved magnetite associated with sulphides (**a**,**b**) from the Perivoli area, Pindos ophiolite complex. Abbreviations as in Figure 3.

3.1.4. Massive Magnetite in Mafic Ophiolitic Rocks Edessa (Samari)

The isolated ophiolite masses of Eastern Edessa belong to the Axios zone (Almopias subzone) [25–27]. At the area of Samari, Edessa, with dominant rock types diabase, gabbros, and serpentinized peridotites, ore bodies consisting of magnetite separates and sulphides have been described [27]. Magnetite occurs (1) as disseminated euhedral and/or subhedral crystals, along with sulphides (pyrite, chalcopyrite) within gabbros and diabase, accompanied by epidote, chlorite, quartz, sphene and tremolite; and (2) as massive ore hosted within gabbros, close to its contact with peridotite, with a gangue silicate mass dominant by greenalite, while sulphide veinlet crosscutting the magnetite separate ore are common (Figure 5) [27]. The magnetite is pure, characterized by the presence of only negligible contents of other elements (Table 1).

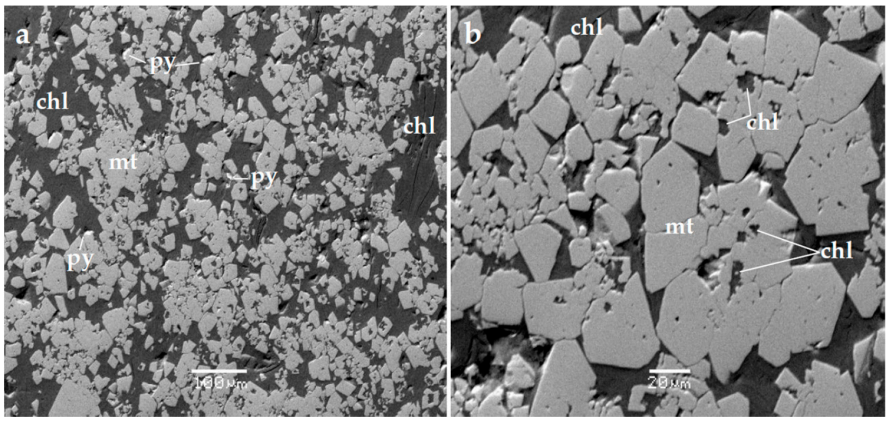

Figure 5. Back-scattered electron (BSE) images showing massive magnetite associated with little amounts of pyrite in a matrix of chlorite (greenalite) (**a**) and inclusions of chlorite in magnetite (**b**) from the Samari area (E. Edessa). Abbreviations as in Figures 2 and 3.

3.1.5. Massive Magnetite Associated with Apatite in Ophiolites

Major Mesozoic ophiolite complexes in Greece, including the Othris, Pindos, and Vourinos suites, were all obducted from the Middle-to-Late Jurassic and have been interpreted as parts of the same oceanic slab, although fore-arc and back-arc ridges have been tectonically fragmented and separated by overlapping sediments [28,29]. The Othrys ophiolite complex consists of a stack of thrust sheets in which overlapping stratigraphic successions, consisting mainly of harzburgites, lherzolites, gabbros, mafic dikes, and pillow lavas, have been recognized, while small irregularly shaped bodies of gabbro and gabbroic dikes or veins intrude the plagioclase lherzolite of the mantle sequence [30]. Irregular to lens-like occurrences (0.5 m × 1 m) of massive pure magnetite associated with large (up to 3 cm long) well-formed crystals of chlor–hydroxyapatite apatite, and lesser amounts of serpentine, tremolite, and Ni silicates (nepouite, pimelite), and by Ni sulfides (pentlandite, violarite, heazlewoodite) have been described in the Agoriani area of the Othrys ophiolite complex, central Greece [31]. The analysis of magnetite separates showed very little Al, Mg, Ni, Ti, and REE content (Table S1).

3.2. Magmatic Magnetite Separates

3.2.1. Disseminated Magnetite in Ultramafic Lavas and Wherlites

The Agrilia formation, Othrys ophiolite complex, about 6 km Northwestern of Lamia, is an unusual ultramafic lava characterized by high Mg content (31–33 wt.% MgO) [32]. Olivines from the Agrilia ultramafic lavas display high forsterite (Fo) contents, and calculated parental magma (in equilibrium with $Fo_{90.5}$) approximately 17 wt.% MgO [33]. Disseminated chromite occurs within groundmass (devitrified glass) and as inclusions in olivine and clinopyroxene [32–35]. The chromite spinel within groundmass is commonly rimmed by Ti–magnetite with sharp contacts (Figure 6a). Chromite is Cr-rich, exhibiting a limited range of variation (Table 3). Amphibole (tschermakite after [34], rhönite, chromite, and Ti–magnetite all associated with groundmass (Figure 6)). Rhönite in association with Ti–magnetite within devitrified glass (Table 3), and inter-grown with amphibole, may be of genetic significance [33,34]. The above ultramafic lavas are associated with medium-to-coarse grained wehrlite. They are mainly composed by olivine, clinopyroxene, hornblende, and in lesser amounts, spinel, orthopyroxene, phlogopite, and magnetites.

Table 3. Representative electron SEM/EDS analyses of rhönite (Rho) and amphibole (amph) within devitrified glass (Figure 6) from the Agrilia ultramafic lavas [35]. Symbol n.d. = no detected.

Host	**Devitrified Glass (d.G.)**							
	Rhonite (Rho)			d.G.		Amphibole (amph)		
SiO_2	26.3	26.6	25.8	33.1	45.6	39.8	40.4	55.2
MgO	8.8	8.7	8.8	14.5	6.5	9.2	10.6	11.1
Al_2O_3	15.7	14.9	15.2	12.1	9.9	16.5	17.5	10.6
Cr_2O_3	n.d.	n.d.	n.d.	0.8	1.1	n.d.	n.d.	1.3
CaO	10.7	10.6	10.6	4.3	3.1	10.1	9.6	10.4
TiO_2	4.9	3.9	4.7	1.6	0.2	1.9	1.2	0.2
FeO	28.9	29.8	30.3	27.1	21.8	17.7	17.1	6.2
MnO	0.2	0.2	0.3	0.2	0.2	n.d.	0.3	n.d.
Na_2O	0.5	0.5	1.3	1.6	6.9	2.5	1.7	2.7
K_2O	n.d.	n.d.	n.d.	0.2	0.9	0.3	0.2	0.3
NiO	n.d.	n.d.	n.d.	n.d.	n.d.	n.d.	n.d.	n.d.
Cl	n.d.	n.d.	n.d.	n.d.	n.d.	0.2	0.2	n.d.
Total	96.0	95.2	97.0	95.5	96.2	98.2	98.8	98.0

3.2.2. Disseminated Magnetite Separates in Norite Gabbros (Central Vourinos, Krapa Hills)

The Vourinos ophiolite complex located in NW Greece constitutes a complete but tectonically disrupted ophiolite sequence. Two magmatic series have been preserved at the central part of the complex, which constitute the earlier Krapa sequence, consisting of magnetite-bearing gabbro-norite

and leuco-gabbro-norite (minor magnetite-bearing) and the younger Asprokambo sequence [36]. The Fe–Ti mineralization occurs as disseminated grains in a proportion of 5–20 vol.% between coarse-grained clinopyroxene and plagioclase, while sulphides (pyrrhotite, pyrite, chalcopyrite) are present in lesser amounts. Ti–magnetite occurs as interstitial to the major phases as small disseminated euhedral and irregular grains (Figure 7). Ti-bearing magnetite separates exhibits low Si, Mg, and high Al (1.7–2.3 wt.% Al_2O_3), Ti (3.5–6.9 wt.% TiO_2), and V (1.4–2.1 wt.% V_2O_5 contents) (Table 1).

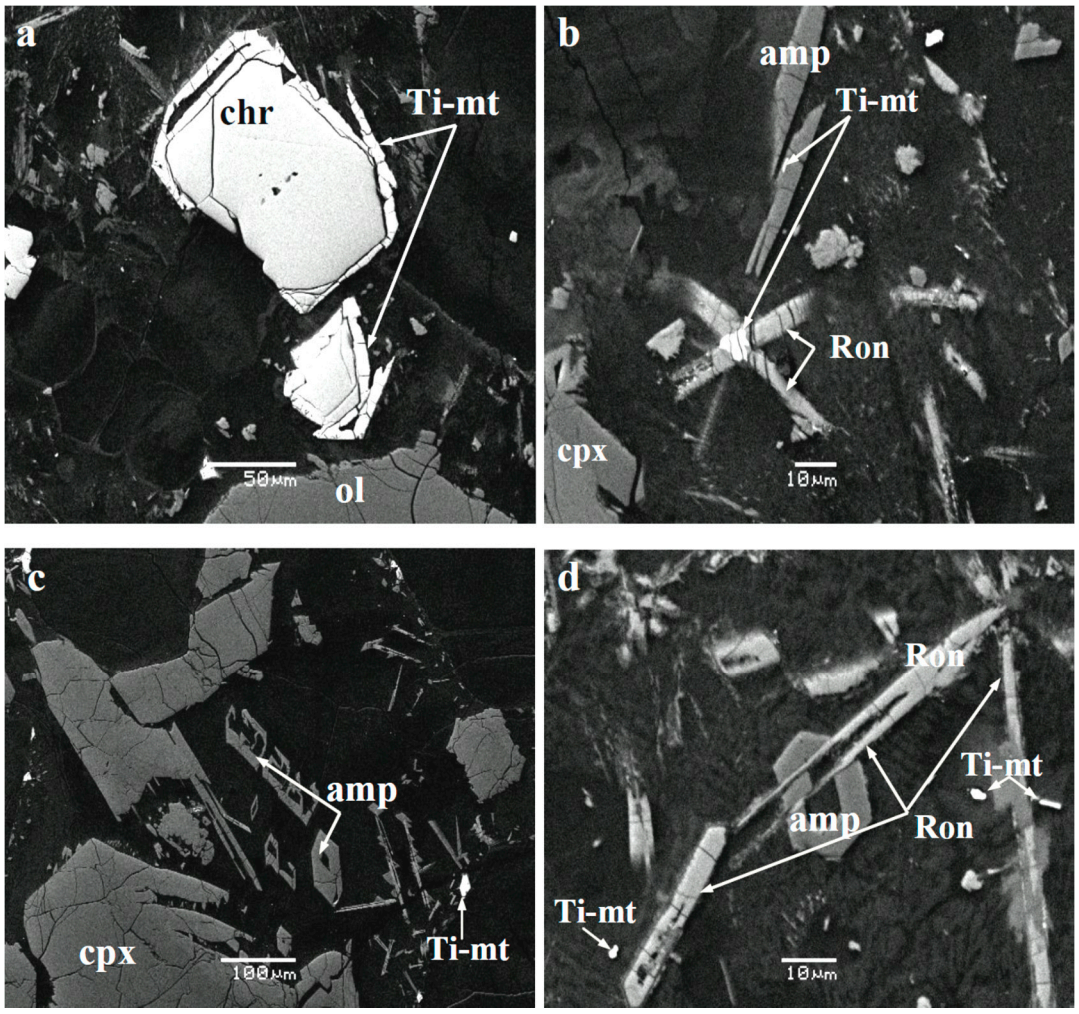

Figure 6. Back-scattered electron (BSE) images from ultramafic lavas of the Agrilia Formation, showing the association of Ti–magnetite (Ti–Mt) with chromite (chr) (**a**), microcrystals of rhönite (Ron) (**b**) associated, and randomly oriented amphibole (Amp) (**c**,**d**).

3.3. Magnetite in Coastal Black Sand

The volcanic rocks of the South Aegean arc form a chain from the Saronikos Gulf in the west, to Kos, Nisyros, and the east, through the Milos and Santorini islands [37]. Multiple eruptions of calc-alkaline to tholeiitic composition and Plio-Pleistocene age are located from the Santorini toward the Nisyros–Kos volcanic rocks (Figure 1a) [37–39]. Those volcanic rocks are part of the volcanic system related to the northward subduction of the last remnant of the oceanic crust of the African plate beneath the southern edge of the active margin of the European plate [38–41]. Magnetite and other heavy minerals have been found in all volcanic types in small quantities (1–2 modal %).

The investigated coastal black sand samples (black sea sand) collected from the Northern part of Kos Island revealed the presence of abundant Ti–magnetite with inclusions of apatite, ilmenites, Fe–Mn-oxides and monazite [(Ce, La, Th, Nd, Y) PO_4] (Figure 8). Feldspars and quartz are common too.

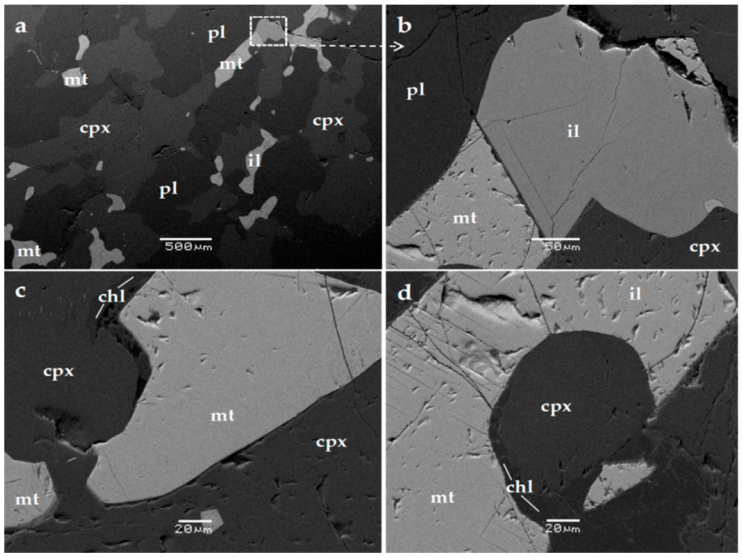

Figure 7. Back-scattered electron (BSE) images from the gabbro-norite sequence of Central Vourinos (Krapa area) showing disseminated Ti–magnetite as small euhedral and irregular phase associated with ilmenite (il) interstitially to the major phases of clinopyroxene (cpx) anf plagioclase (pl) (**a**–**d**).

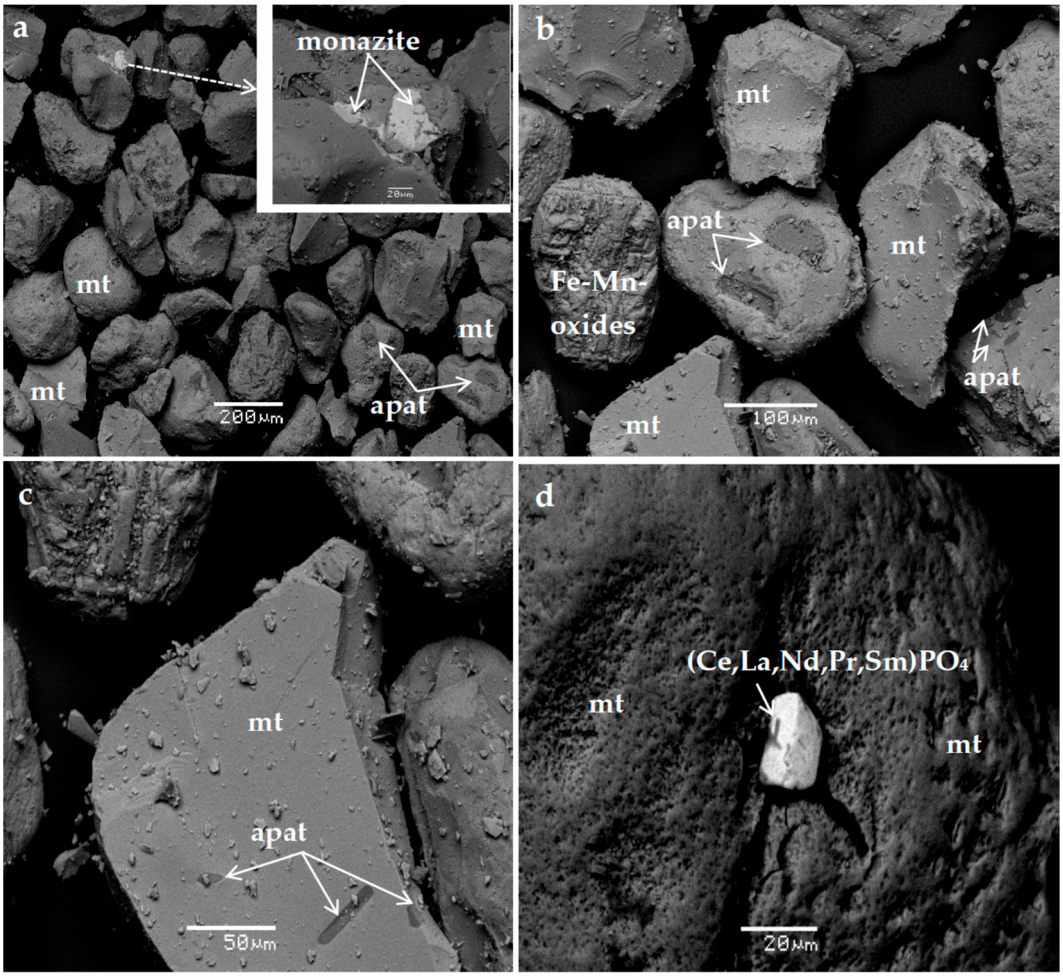

Figure 8. Back-scattered electron (BSE) images of coastal black sand collected from the northern part of Kos Island, showing that Ti–magnetite is the dominant oxide, while apatite (apat) forms inclusions of approximately 100-μm-long grains (**a**–**c**); Fe–Mn-oxides (**b**), monazite [(Ce, La, Th, Nd, Y) PO_4 and (Ce, La, Nd, Pr, Sm) PO_4] are common (**a**,**d**).

The sample from the Nisyros caldera (neighboring Kos Island) comes from whitish extinct fumaroles co-existing with native sulphur, that is dominant by opal (Figure 9). The analyzed sample of the formation from the Nisyros caldera is opal–CT and quartz [41], which it is associated with abundant native sulphur (Figure 9).

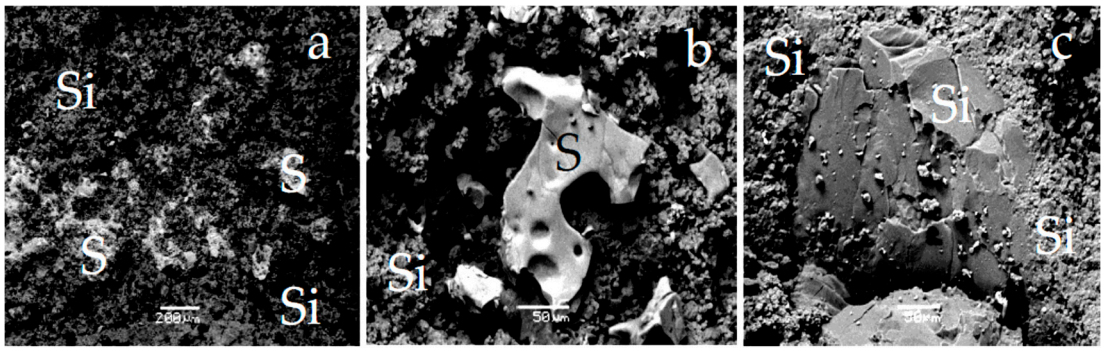

Figure 9. Back-scattered electron (BSE) images (unpolished sections) of extinct fumarole formation from the hydrothermal crater of the Nisyros caldera, showing native sulphur (**a**,**b**) and the association of native sulphur with whitish Si material (opal) (**c**), having low REE content (Table S1).

3.4. Magnetite Separates from Metamorphosed Fe–Ni-Laterites (Olympos, Edessa, and Vermion)

The dismembered ophiolite masses of the Olympos, Edessa, and Vermio mountains (Upper Jurassic–Lower Cretaceous), composed mainly by serpentinized harzburgite and, to a lesser extentm crustal magmatic rocks (pyroxenites and gabbros), outcrop along the eastern margin of the Pelagonian massif. They are considered to have been derived from the Almopias subzone of the Vardar zone and were overthrust westward onto the Pelagonian massif [22]. They are mostly composed of a mantle sequence (harzburgites) and crustal magmatic rocks, both characterized by supra-subduction zone (SSZ) features [23]. Small laterite bodies are located in the Olympos, Edessa, and E. Vermio Mountains, at the contact of serpentinized harzburgites with Upper Cretaceous limestones or within the serpentinites themselves. Due to intense tectonism, the Fe–Ni-laterite occurrences are often entirely enclosed within serpentinized harzburgites [1,25]. Apart from fine-grained magnetite separates in the matrix of the Fe–Ni ore, magnetite separates are associated with chromite, as the product of a gradual alteration of chromite or epitaxial as rims on chromite (Figure 10). A salient feature of zoned chromite grains from the Olympos, Edessa, and Vermion laterite occurrences is a Cr, Al, and Mg gradual decrease as Fe increases outward from the core; Mn, Zn, and Co increases gradually outwards, attaining greatest values at the periphery of chromite cores and in the Fe–chromite, up to 13.0, 2.1, and 4.1 wt.%, respectively, and drops off to negligible values in magnetite separates (Table 4). At the area of Vermio, there is abundant garnet (grossularite) and calcite, while Ni is mainly hosted in chlorite, serpentine, and theophrastite containing 80 wt.% NiO (Figure 10; Table 4) [42]. A (Co, Mn, Ni)-hydroxide with a wide compositional range occurs in a spatial association with theophrastite (Figure 11; Table 4) [43]. Several SEM-EDS analyses of hydroxides can be classified into two groups (Figure 11): Group A includes phase mineral dominated by cobalt, and group B those dominated by Mn, towards the peripheral parts of the concentrated development (Figure 10).

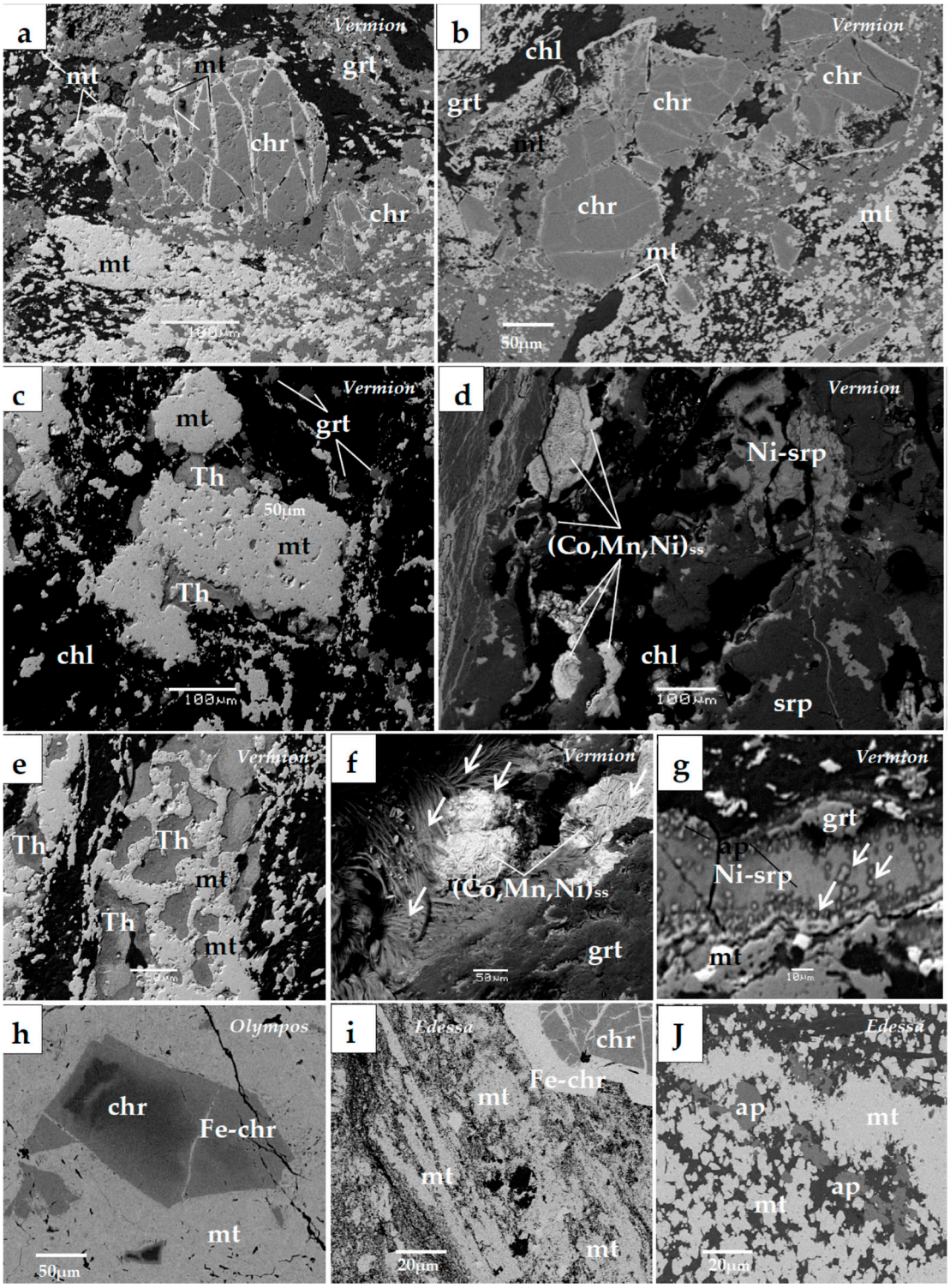

Figure 10. Back-scattered electron (BSE) images of metamorphosed Ni-laterites from northern Greece. Magnetite (mt) surrounding chromite (chr) grains and occurring along cracks (**a**,**b**,**e**,**f**); various morphological forms and textural relationship between magnetite–theophrastite (Th) and garnet (grt) (**c**,**f**,**g**); magnetite crosscutting veinlets (**e**,**i**,**j**); magnetite–(Co–Mn–Ni)$(OH)_{ss}$ showing successive thin layers, composed by fine fibrous crystals (**d**); microtextures resembling fossilized microorganisms coated by (Co–Mn–Ni)$(OH)_{ss}$ (white arrows) (**f**) or isolated and aggregates of bacterio-morphic Fe–Ni–serpentine (white arrows) within a veinlet of Ni–serpentine (Ni–srp) (**g**); chromite–Fe–chromite (**h**); chromite–magnetite (**i**); magnetite–apatite (ap) (**j**).

Table 4. Representative electron SEM/EDS analyses of chromite cores, magnetite (mt) and Fe–chromite (Fe–chr), Theophrastite and (Co, Mn, Ni)-hydroxides from Ni-laterites of the Vermion mountain (Northern Greece; Figure 10). Symbol n.d. = no detected.

	Olympos					**Edessa**			**E. Vermion**			
Location	Paliambela					Nissi	Mavrolivado			Stournari		
Mineral	Core Chromite	Fe-chr	Rim mt	Core Chromite	Fe-chr	Rim mt	Core Chromite	Fe-chr	Rim mt	Theophastite	(Co,Mn,Ni)-hydroxides		
sample	L1	L1	L1	Ed10	Ed10	EdP10	V.AK	V.AK	V.AK				
wt.%													
SiO_2	0.2	n.d.	0.4	n.d.	n.d.	0.5	0.3	0.7	1.2	n.d.	n.d.	n.d.	n.d.
Al_2O_3	8.2	8.6	0.4	9.7	6.5	0.2	24.4	7.7	0.5	n.d.	n.d.	n.d.	n.d.
Cr_2O_3	62.1	53.7	5.9	60.2	58.1	1.6	43.3	42.3	1.6	n.d.	n.d.	n.d.	n.d.
Fe_2O_3	1.8	3.5	62.2	2.7	3.3	67.7	2.2	17.6	66.5	n.d.	n.d.	n.d.	n.d.
FeO	13.9	27.6	28.4	15.5	8.3	29.3	17.3	26.6	28.9	1.0	n.d.	n.d.	n.d.
MgO	11.3	0.6	0.4	11.2	3.5	0.3	11.1	2.2	0.3	n.d.	n.d.	n.d.	n.d.
MnO	1.9	4.1	0.5	1.6	13.1	n.d.	n.d.	2.8	0.3	n.d.	25.0	13.9	19.2
ZnO	n.d	0.4	n.d.	n.d.	2.1	n.d.	0.5	0.7	0.3	n.d.	n.d.	n.d.	n.d.
CoO	n.d.	n.d.	0.4	n.d.	4.1	n.d.	n.d.	n.d.	n.d.	n.d.	38.0	54.3	46.9
TiO_2	n.d.	n.d.	n.d.	n.d.	n.d.	n.d.	n.d.	n,d.	n.d.	n.d.	n.d.	n.d.	n.d.
NiO	n.d	n.d.	1.6	n.d.	n.d.	1.4	n.d.	0.2	n.d.	79.2	17.4	11.2	13.6
Total	99.4	98.5	100.2	100.9	99.0	101	99.1	100.8	99.6	80.2	80.4	79.44	79.7
Cr/(Cr + Al)	0.83	0.81	0.81	0.78	0.86	0.87	0.54	0.79	0.94				
Mg/(Mg + Fe^{2+})	0.55	0.03	0.13	0.47	0.17	0.01	0.51	0.12	0.01				

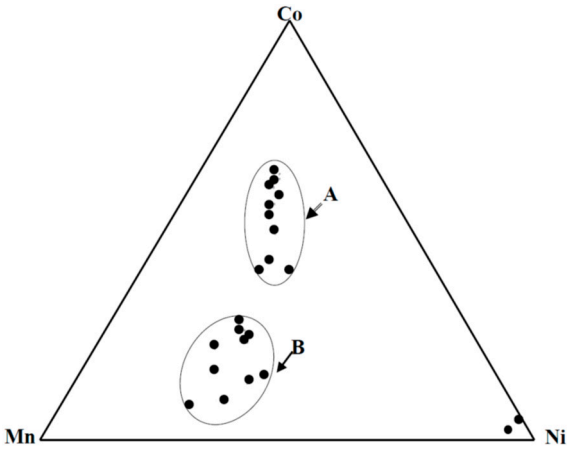

Figure 11. Triangular plot of Co, Mn, and Ni (atom%) showing the compositional variation of the (Co, Mn, Ni)$_{\text{solid solutions}}$ [43].

The (Co, Mn, Ni)$_{\text{solid-solution}}$ phases are associated with theophrastite, pyrochroite, Ni–serpentine (garnierite), garnet (grossularite), and magnetite, all having a common origin, subsequently of the strong late tectonic evolution, overprinting earlier deformation events (Figure 10c–g). They occur as successive thin (a few to tens of μm layers, composed by fine fibrous crystals up to a few μm (Figure 10d), microtextures resembling fossilized microorganisms coated by (Co–Mn–Ni) (OH)$_{ss}$ (white arrows) (Figure 10f), or isolated and aggregates of bacterio-morphic Fe–Ni–serpentine (white arrows) within a veinlet of Ni–serpentine (Ni–srp) (Figure 10g).

4. Geochemical Characteristics of Magnetite Separates

Although a good separation of magnetite from very fine inter-grown silicates and/or sulphides (Figures 2–10) was not achieved, it is clear that the highest Cr, Mn, and Co contents were recorded in Fe–Ni-laterite occurrences of northern Greece, ranging from 1.1 wt.% Cr in Vermio to 9.0 wt.% Cr in Olympos, from 0.38 wt.% Mn in Vermio to 0.69 wt.% Mn in Olympos, and from 460 ppm Co in Olympos to 1060 ppm Co in the Edessa laterites (Table S1).

The highest Ti and V contents were determined in disseminated magnetite separates from the magmatic sequence (norite gabbros) of the Vourinos (Krapa) ophiolite complex (2.56 wt.% Ti, 6330 ppm V), the Agrilia ultramafic rocks from the Othrys complex (7.48 wt.% Ti, 1760 ppm V), and the coastal black sands (or placer deposits) from Kos Island. In addition, magnetite separates from the Agrilia ultramafic rocks is richer in Al, Mg, Ti, and Cr compared to that from the Krapa norite-gabbros. Magnetite separates from the Skouries deposit shows relatively significant contents of Ni (up to 640 ppm Ni) and Cr (up to 1060 ppm Cr) (Table S1).

Hydrothermal magnetite separates from the ancient Lavrion (Plaka) mine, that is of skarn-type, and the Skouries porphyry deposits, that is disseminated, both associated with calc-alkaline rocks differ in terms of the higher Ba, Bi, Cr, Ni, Co, V, Sr, Sc, Rb, ΣREE, Y, Hf, Th, U, and Zr contents in the latter (Table S1). Gallium is higher in magnetite separates associated with cal-alkaline rocks (38–59 ppm) compared to that associated with ophiolites (2–21 ppm Ga) (Table S1). The highest Ga contents were recorded in magnetite separates from the Skouries porphyry-Cu deposit (40–59 ppm), skarn-type from Lavrion mine (38–39 ppm), and coastal sand from Kos Island (42 ppm), all related with calc-alkaline rocks. A potential order of the average Ga content in magnetite separates, from low to high is from Ni-laterites, hydrothermal (ophiolites) associated with sulphides, ultramafic lavas (ophiolites), hydrothermal (ophiolites) associated with apatite, magmatic (norite-gabbros), skarn-type (calc-alkaline), coastal sands (calc-alkaline volcanic), and porphyry-Cu deposits (hydrothermal calc-alkaline), resulting into a discrimination using a plot of (V + Ti) versus Ga content (Figure 12).

The rare earth element (REE) content of the majority of hydrothermal magnetite separates analyzed, such as those from the Lavrion mine (skarn-type), the Skouries porphyry-Cu deposit, the Pindos

(Perivoli) and Edessa (Samari) is generally low (a few decades ppm and REEs exhibit similar trends. Although the REE content, as well as actinides (Th, U) and Zr, in the porphyry (Skouries) deposit are higher compared to those in skarn-type (Lavrion), the REE patterns are similar in terms of the negative Eu, Tm, and Ho anomalies, but the former display occasionally positive Eu anomalies as well, and slight negative anomalies in Sm and Tm (Figure 13a,b). Moreover, considering the magnetite separate samples from the Skouries deposit, it seems likely that there is a small increase of the REE_{total} with the increasing depth from 43 to 363 m. In addition, the magnetite separate sample from the lowest depth (43 m) exhibits a positive Eu anomaly, in contrast to the samples from deeper parts of the deposit (Figure 13; Table S1). The hydrothermal magnetite separates associated with apatite from the Othrys (Agoriani) complex show higher REE content (54 and 80 ppm), that is, increasing with the presence of apatite, reaching values to more than 1300 ppm REE in apatite [31].

Calculations of Ce, Eu, Pr, and Gd anomalies were defined [44] by equations such as: Ce/Ce* = (2Ce/Ce chondrite)/(La/La chondrite + Pr/Pr chondrite) and Eu/Eu* = (2Eu/Eu chondrite)/(Sm/Sm chondrite + Gd/Gd chondrite). Assuming that values > 1 and < 1 are called positive and negative anomalies, respectively, chondrite normalized REE patterns for Ni-laterites from the Vermio mountains showed negative Ce, Eu anomalies, which is in agreement with the Ce/Ce* (0.56–0.24) and Eu/Eu* (0.40–0.24) values (Table S1). The highest REE contents were recorded in Ti–magnetite separates from the ultramafic lavas (130 ppm) and from the coastal sands, Kos Island (220 ppm). Sulphur occurs to be impregnated with particles of rocks, including opal–CT, quartz, alunite, anhydrite, and kaolinite (Figure 9) [41]. There is enrichment for light rare earth elements (LREE) from La to Sm and decrease for the heavier REE in magnetite separates compared to andesitic volcanic rock from Santorini Island (Figure 13f), and enrichment for all REE compared to the recent formation, associated with abundant native sulphur in Nisyros Island (Figure 9a,b). A distinct negative Eu anomaly is a common feature of the magnetite separates from the coastal sand of Kos and the andesitic rock from Santorini Island.

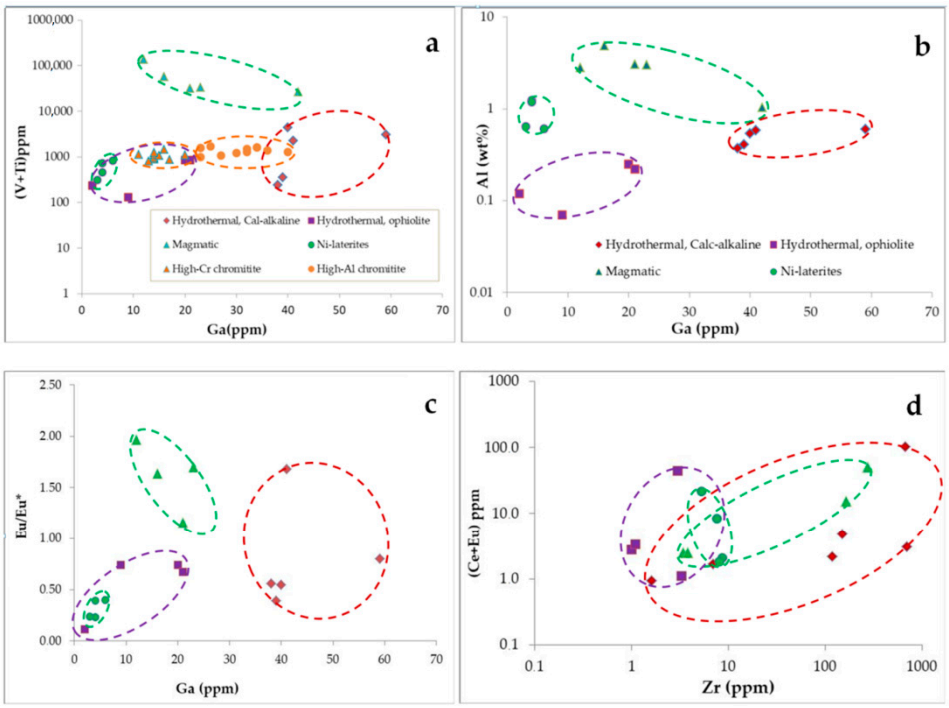

Figure 12. *Cont.*

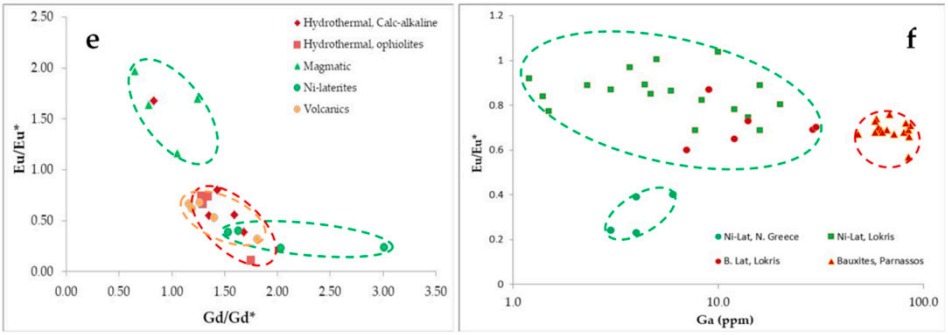

Figure 12. Plots of (V + Ti) and Al versus Ga contents (**a**,**b**), Eu/Eu* ratio versus Ga content (**c**); (Ce + Eu) versus Zr content (**d**), Eu/Eu* versus Gd/Gd* ratios (**e**), all for magnetite separates (data from Table S1) and plot of the Eu/Eu* ratio versus Ga content for Fe–Ni-laterites from Northern and Central Greece (Ni-lat), bauxite latererite (B-lat), and bauxites from Parnassos-Giona zone (**f**). Data from Table S1 and literature [45,46].

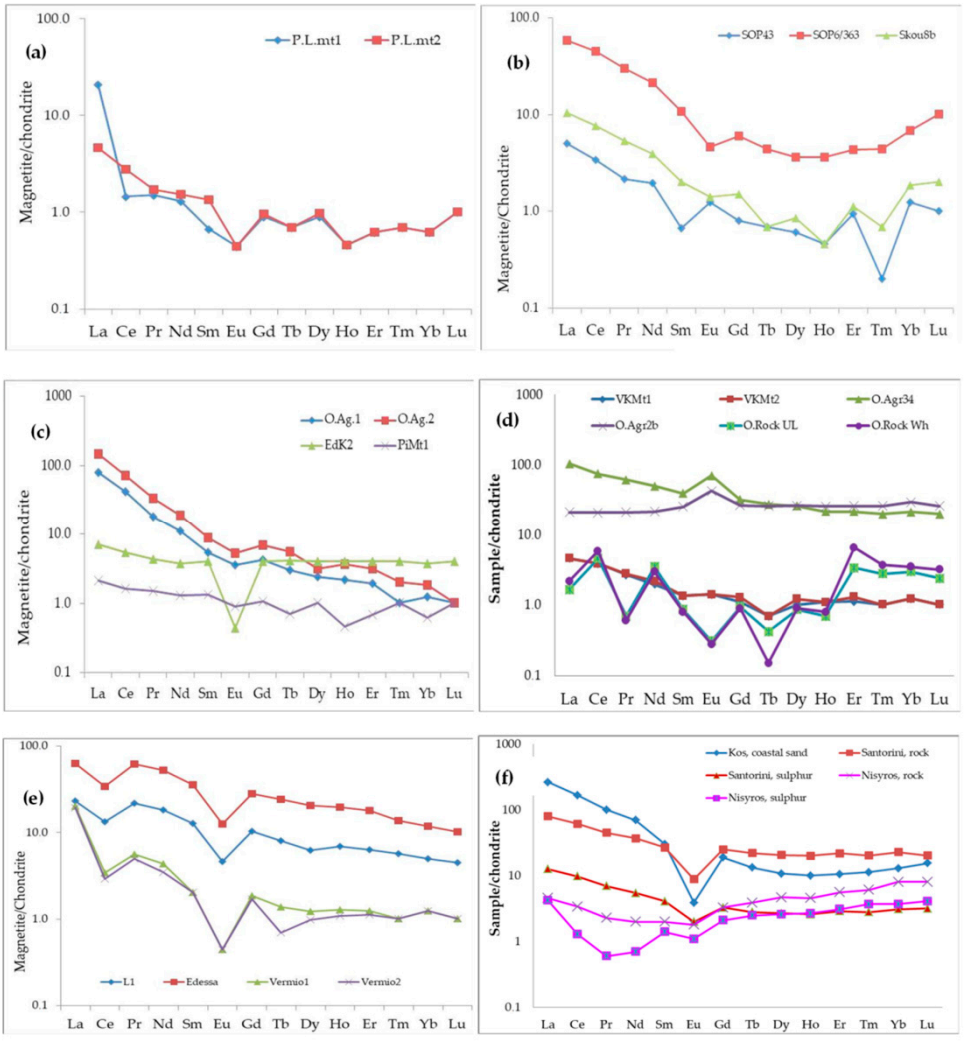

Figure 13. Chondrite normalized diagrams for magnetite separates (**a**–**f**) and volcanic rock (**d**,**f**). Data from Table S1 and [47] for ultramafic lavas (sample labeled as Rock UL, $n = 3$, and wehrlite (Wh), $n = 7$) from the Othrys ophiolite complex. Chondrite values from McDonough and Sun [48].

Moreover, the same trace elements were analyzed in two samples representing extinct fumaroles of andesitic and rhyolite composition, co-existing with native sulphur from the Aegean active volcanic

arc, collected from Santorini (andesite) and Nisyros Island (Figures 9 and 13f). There is enrichment of LREE from La to Sm and decrease of the heavier REE in magnetite separates from costal sands (Kos), that is comparable to andesitic material from Santorini Island (Figure 13f). In addition, they exhibit elevated REE content compared to the extinct fumarole from Nisyros Island (Table S1; Figure 12f). Furthermore, REE patterns of both extinct fumarole material and native sulphur from Nisyros differ in terms of the low LREE content, the relative HREE enrichment compared to magnetite separates and andesitic material from Santorini and the negative Ce, Pr, and Eu anomalies (Figure 13f; Table S1).

Relatively high REE contents were recorded in Ti–magnetite separates from the ultramafic lavas from the Agrilia (99 ppm), while in wehrlite it is only 23 ppm. However, both are clearly higher compared to ultramafic lavas and wehrlite rocks (literature data), ranging from 14 to 17 ppm REE_{total}, respectively [47]. Chondrite normalized REE for magnetite separates from ultramafic lavas and wehrlite display sub-parallel patterns, with slight LREE enrichment in ultramafic lava, and an inverse relationship in terms of heavy rare earth elements (HREE) (Figure 13d). The Eu content in Ti–magnetite separates from the ultramafic lavas of Agrilia (Othrys) is enriched, showing a positive anomaly; in contrast, it is depleted in the magmatic sequence (norite gabbros) of the Vourinos (Krapa) complex (Figure 13d). In addition, the REE patterns for ultramafic lavas and wehrlites (literature data [47]) show a slight HREE enrichment for wehrlites compared to ultramafic lavas too (Figure 13d), while both rock types exhibit clear positive Ce, Nd, Gd, and Er anomalies and negative Pr, Eu, and Tb anomalies (Figure 13d).

In summary, the analyzed samples of magnetite, both massive ore and separates, covering a wide range of associated rock type, reveal wide compositional variations (Table S1 and Table 5). Although much compositional overlaps were recorded, a potential classification of magnetite separates is: (a) Magmatic: (a1) Associated with ophiolites and (a2) associated with calc-alkaline volcanic rocks (coastal sands); (b) hydrothermal: (b1) Associated with ophiolites and (b2) associated with calc-alkaline rocks (skarn-type and porphyry-Cu–Au deposits); and (c) epigenetic origin of magnetite separates in laterites (Figures 2–13). Average values show the highest ΣREE contents in disseminated magnetite separates from ultramafic lavas (Othrys) and coastal black sands (Kos Island) (Table 5).

Available data from previous publications have shown that an enrichment in Cr and Ni is a common feature of porphyry-Cu–Au–Pd–Pt, such as the Skouries, Elatsite, and other porphyry deposits worldwide, characterized by significant Pd and Pt contents, in contrast to the porphyry-Cu ± Mo deposits of Russia and Mongolia with lower Pd–Pt content (Figure 14) [4,12–14,49].

Table 5. Summary of the certain trace element contents (ICP-MS analyses) in magnetite separates and/or host ores.

MAGMATIC	Location	Rock-Type	Texture	ΣREE	Ce/Ce*	Eu/Eu*	Pr/Pr*	Gd/Gd*	Ga	V	Ti	Cr	Ni	Reference
Ophiolites	Vourinos (Krapa)	Norite gabbro	Disseminated	6	1.06	1.43	0.92	1.14	22	6520	2.6	1070	100	Present study
	Othrys	Ultramafic lava	Disseminated	132	0.9	1.97	0.98	0.65	12	1820	13.4	1600	160	Present study
Calc-alkaline	Kos	Coastal sand	Placer	224	0.92	0.32	0.85	1.81	42	1480	2.5	1150	11	Present study
HYDROTHERMAL														
Ophiolites	Edessa (Samari)	Peridotite	Massive	10	0.94	0.11	0.95	1.75	2	34	0.02	560	56	Present study
	Othrys (Agoriani)	Association with apatite	Massive	76	0.82	0.70	0.71	1.28	20	640	0.02	1100	280	Present study
	Pindos (Perivoli)	Irregular	Massive	3.1	0.90	0.74	1.02	1.34	9	80	<0.01	12	6	Present study
Calk-alkaline	Skouries	Porphyry-Cu	Disseminated	26	0.98	1.01	0.88	1.20	46	760	0.25	630	340	Present study
	Lavrion (Plaka)	Skarn	Massive	3	0.81	0.48	0.94	1.64	3.9	44	0.02	160	30	Present study
METAMORPHOSED	Olympos,Vermio, Edessa	Ni-laterites (n = 4)	Major, matrix	37	0.41	0.32	1.45	0.93	4.2	280	380	33,980	9800	Present study
Fe-Ni-laterite	Lokris	Ni-laterites (n = 13)	Rare, matrix	120	1.02	0.85	0.96	1.14	7.6	75	2900	1900	2200	[46]
Bauxite laterite	Lokris	Bauxitic laterites (n = 6)	Rare, matrix	350	1.01	0.71	0.97	1.2	17	340	7200	3500	1400	[46]
Bauxite	Parnassos-Giona	Bauxites (n = 17)	Rare, matrix	470	2.64	0.69	0.58	0.8	70	460	16,000	820	150	[45]

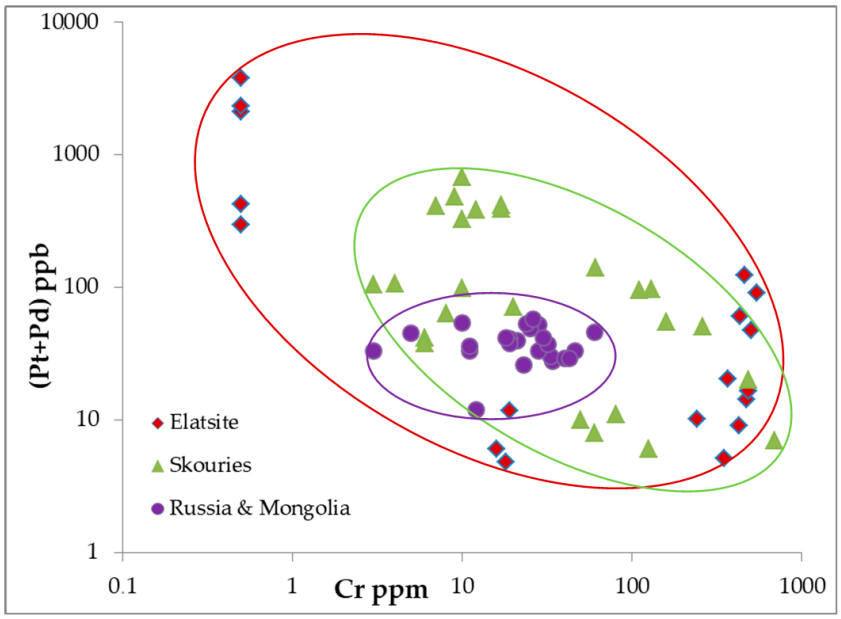

Figure 14. Plot of the (Pt + Pd) versus Cr content in porphyry-Cu–Au–Pd–Pt and porphyry-Cu–Mo deposits. Data from literature [12,14,49].

5. Discussion

The trace element content in magnetite separates, coupled with mineral chemistry and texture relationships, may provide evidence on (1) their parent magma or hydrothermal ore forming system, (2) partition coefficient of trace elements into magnetite separates, and (3) physico/chemical conditions (temperature, fO_2) during deposition and/or re-deposition of magnetite separates, and can be used as a prospective tool for many types of ore deposits [5–10,50]. The recorded wide variations in the trace element contents of massive and concentrates of disseminated magnetite separates from Greece may be used to discriminate between magmatic and hydrothermal magnetite separates, associated either with calc-alkaline rocks and ophiolites, between porphyry-Cu + platinum-group elements (PGEs) and porphyry-Cu lacking precious metals deposits, and between laterite types.

5.1. Trace Element Distribution in Magnetite Structure and Associated Minerals

The geochemistry of magnetite separates is affected by a variety of cations accommodated in the spinel-type structure [3,14,15] and the co-precipitation of other minerals [5–10]. The high-resolution studies of minerals applying TEM techniques provide a new and very important way to elucidate valuable information on the physico/chemical processes and mechanisms during formation of ore deposits and post-depositional changes of ore minerals [51]. The investigation of hydrothermal magnetite separates from the Los Colorados iron oxide–apatite deposit in Chile showed three generations of magnetite, which vary significantly in terms of their Si, Al, Ca, Mg, Ti, Mn, Na, and K minor and trace element contents, in contrast to the V content (remarkably constant), and concluded a complex incorporation of trace elements during growth of magnetite [51]. Although, there is a discrepancy between experimentally determined values and those derived from natural occurrences, the partition coefficients for spinel–liquid pairs ($D^{sp/lq}$), for high field strength elements, such as Ga, V, Zr, Zn, and Co, are extremely low [50,52]. Considering the presented data (Table S1), potential components of sulphide (Cu, Zn) and/or silicate (Si, Mg, K) inclusions in magnetite separates are used with caution. Selected elements, such as V, Ti, and Ga, in individual types of magnetite separates are plotted, showing different fields for magmatic and hydrothermal magnetite, and furthermore, between hydrothermal magnetite associated with ophiolites and calc-alkaline rocks (Figure 12).

Hydrothermal apatite from the Othrys (Agoriani) ophiolite complex contain over 1300 ppm ΣREE [31], whereas the associated magnetite separates contain less than 100 ppm ΣREE, due probably to incomplete separation of apatite (low P and Ca contents) (Table S1) [31]. Similarly, magnetite separates from the coastal black sand from Kos, containing inclusions of apatite (Figure 8b,c), exhibit relatively high (over 220 ppm ΣREE) (Table S1) and monazite of varying composition [(Ce, La, Th, Nd, Y) PO_4 and (Ce, La, Nd, Pr, Sm)PO_4] (Figure 8a,d). Magnetite separates from black coastal sands can be linked back to a volcanic source, and may be a potential REE source [41]. On a global scale, in many placer deposits, such as the river placers in Malaysia, paleo-placers in South Africa, Elliot Lake, Ontario, and beach sand deposits in India, monazite is an important REE mineral and many monazite ore deposits are economically important REE resources, although small contents of Th and U make monazite a restricted mineral in India [53]. Also, hydroxyl–bastnaesites and a (La, Nd, Y) (CO_3) F member of the bastnaesite group, which are among the most economically important as well, have been identified at the lowest part of karst-type laterites in Greece, close to their contact with carbonates [54–57].

The first data on magnetite separates from black coastal sand from Kos Island are compared with potential parental rocks of the neighboring active Nisyros Island and Santorini, all belonging to the Aegean volcanic arc, showing REE, Ti, V, Cr, Mn, Zn, and Ga contents in magnetite separates are higher than those in the volcanic rocks of basaltic composition from Santorini Island [50] and Nisyros Island (Table S1). The similarity between the REE patterns, including the clear Eu negative anomaly of magnetite separates from coastal black sand of Kos Island and that of andesitic material from Santorini Island (Figure 13f), may provide evidence of an andesitic source of the placer magnetite separates in Kos. Also, the composition of native sulfur has been used to qualitatively estimate elemental abundances in low-temperature fumarole gases. At low temperatures (<250 °C), oxygen in the atmosphere interacts with H_2S, resulting to precipitation of native sulphur [58].

5.2. Re-Mobilization and Re-Deposition of Magnetite

Magnetite separates as a late magmatic or early hydrothermal phase in both calc-alkaline systems and ophiolite complexes may be dissolved and re-precipitated, due to changes in temperature, salinity, pressure, and fO_2 [51,59–61]. An increase in temperature would enhance the solubility and, consequently, the undersaturation of iron in the fluids [61], leading to dissolution of the primary magnetite separates and formation of the secondary varieties. Thus, primary magnetite may have been re-mobilized during late brittle deformation and motion along the detachments contacts [60]. In general, textural and compositional data for magnetite from nine iron skarn deposits in Canada, Romania, and China have shown that most samples have been re-equilibrated by dissolution and re-precipitation and/or recrystallization [16,51]. These authors concluded that the applicability and reliability of trace element discrimination diagrams may be used with caution where magnetite has been subjected to multiple re-equilibration processes, and that detailed textural characterization must be undertaken in order to evaluate the effects of hydrothermal overprinting events and other re-equilibration processes on the trace element compositions of magnetite.

A peculiarity of the above Fe–Ni-laterite occurrences is the relatively high Cr, Mn, Co, and Ni content in Fe–chromite zones of spinels. The epigenetic mobilization of Fe, Mn, Co, and Ni and their re-deposition is suggested by a significant Mn, Zn, and Co enrichment in Fe–chromite (Table 1) and the abundance of Ni–serpentine (Figure 10; Table 4). The substitution for Mg^{2+} and Fe^{2+} by Mn, Zn, and Co in the chromite lattice resulted to a gradual transformation of chromite to Fe–chromite, while in the magnetite, that is considered to be the final product of this alteration process [1,62] and the above elements drop to negligible amounts (Table 4). Calculations for spinel structures [14,15,63,64] have shown that in normal spinels, there is a tendency for the electrostatic energy to favor the larger ions (Fe^{2+} > Mg^{2+} and Fe^{3+} > Al^{3+}) into the tetrahedral site. Thus, the resulting small expansion of the tetrahedral and octahedral sites hampers the entry of other trace elements in the magnetite separate lattice at low temperatures [65,66]. Besides, the re-mobilization of Fe and re-deposition

of magnetite at low temperature is indicated by its association with (Ni, Fe, Co, Mn)-hydroxides. Specifically, the texture relationships between magnetite, theophastite [$Ni(OH)_2$], and (Co, Fe, Mn, Ni) $(OH)_2$ (Figure 10a–h) suggest a common mineral forming system, along shear zones, subsequently of the strong late tectonic evolution, which overprints earlier deformation events, probably at low temperature, approximately 100 °C [67] and alkaline conditions, as it is suggested by the presence of calcite and the high Ca content in the magnetite separates concentrates (Table S1). Moreover, the association of the (Co, Mn, Ni) $(OH)_2$ solid-solution phases with microtextures resembling fossilized microorganisms coated by (Co–Mn–Ni) $(OH)_2$ (Figure 10f, white arrows) and the occurrence of isolated and aggregates of bacterio-morphic Fe–Ni–serpentine (Figure 10g) suggest the potential effect of microorganisms in the Vermio mineral-forming processes. Currently, much research interest has focused on a consortium of microorganisms of varying morphological forms, producing enzymes, which are considered to be a powerful factor to catalyze redox reactions, and act as nucleation sites for the precipitation of secondary minerals [68–70]. In general, the presence of organic matter and microorganism traces in highly tectonized zones of the metamorphosed Fe–Ni-laterites may suggest direct involvement of microorganisms, and have created appropriate conditions for metal bio-leaching and bio-mineralization. In general karst-type Fe–Ni-laterites, where dominant Fe minerals are goethite ± hematite [54,55,71], may display REE contents ranging from a few decades to thousands of more than 5000 ppm (Table S1) [54], depending on the site of the Ni-laterite samples along vertical profiles and the post-deposition processes affected their composition. The epigenetic mobilization of REE, along with Fe, Mn, Ni, Co, under reducing and acidic conditions and, subsequently, re-deposition under alkaline conditions at the lowest parts of contacts between laterites of Central Greece (Lokris) and carbonate rocks has been well established as well [54–56,71]. Thus, the potential depletion of Ga and Al, and elevated Mn, Co, Zn, and Fe ± REE contents has been recorded in the above large Fe–Ni-laterite deposits, but in small Fe–Ni-laterite occurrences in Northern Greece, strongly transformed during post-magmatic metamorphism, the dominant Fe mineral is depleted magnetite, due probably to their small size, facilitating potential changes during sub-solidus reactions. Therefore, the dominance of magnetite in Fe–Ni-laterite ores is not an encouraging factor for the exploration of Ni sources of laterite-type.

5.3. Implications of the Trace Element Distribution for the Origin of Magnetite Mineralization

Despite the potential re-distribution of trace elements in magnetite separate-bearing deposits, disseminated magnetite separates from mafic–ultramafic magmatic rocks of ophiolite complexes exhibit much higher Ti and V contents compared to hydrothermal magnetite, and they are comparable to magnetite separates from coastal sands derived from the weathering of calc-alkaline volcanic rocks (Table 5). The massive hydrothermal magnetite separates of skarn-type differs from the disseminated magnetite separates from porphyry deposits, in terms of the lower Ba, Bi, Cr, Ni, Co, V, Sr, Sc, Rb, ΣREE, Y, Hf, Th, U, and Zr contents (Table S1). Also, Ga is higher in magnetite separates associated with calc-alkaline rocks (38–59 ppm) compared to that related to ophiolites (2–21 ppm Ga) (Table S1). The highest Ga contents were recorded in magnetite separates from the Skouries porphyry-Cu deposit (40–59 ppm), skarn-type from Lavrion mine (38–39 ppm), and coastal sand from Kos Island (42 ppm), all related with calc-alkaline rocks. A potential order of the average Ga content in magnetite separates concentrates, from low to high, is from Ni-laterites, hydrothermal (ophiolites) associated with sulphides, ultramafic lavas (ophiolites), hydrothermal (ophiolites) associated with apatite, magmatic (norite gabbros), skarn-type (calc-alkaline), coastal sands (calc-alkaline volcanic), and porphyry-Cu deposits (hydrothermal calc-alkaline), resulting in a discrimination using a plot of (V + Ti) versus Ga content (Figure 12).

Magnetite separates associated with Fe–Cu–Ni–Co sulphides with dominant minerals pyrrhotite, chalcopyrite, and pentlandite exhibit relatively high Cu and Zn, due to incomplete separation from the associated sulphides, but it is REE-, Ti-, and V-depleted. Although an originally primary magmatic origin for these sulphides is not precluded, characteristics of the highly transformed pure magnetite

separates (Table 1 and Table S1) at Pindos may indicate that potential original magmatic features have been overprinted by a low-level hydrothermal circulation process.

The plot of the Eu/Eu* ratio versus Ga content shows a less negative anomaly Eu/Eu* (average 0.85) for large Fe–Ni-laterite deposits [56,72,73], bauxite laterites and bauxites (63 and 0.69, respectively) [74], and the most negative Eu/Eu* anomaly (average 0.32), for the magnetite separates from Fe–Ni-laterites of Northern Greece (Figure 12e; Table 5). Assuming that the presence of Eu anomaly, caused by the ability of Eu to exist in either Eu^{2+} or Eu^{3+} states, the Eu/Eu* anomalies seem to be effected by physico/chemical conditions, such as a redox potential [74]. Diagenetic re-mobilization of Eu is possible under conditions of reduction to Eu^{2+} at low oxidation potential, as is suggested by the presence of organic matter [73–76]. In addition, the increasing order of the average Ga content from the Fe–Ni-laterites to bauxite laterites and bauxites (Table 5; Figure 12e) is in agreement with the preference of Ga to high-Al ores. The average Ga content for karst bauxite deposits is 58 ppm with a range from less than 10 to 812 ppm, because the close geochemical affinity of Ga to Al enables Ga to substitute easily in rock-forming alumino-silicates [77]. Such a preference Ga with high-Al chromitites, as well and the structural incorporation of Ga into chromite lattice, is evidenced by the progressive and linear increase of Al or decreasing Cr/(Cr + Al) atomic ratio [78,79].

5.4. Implications of Magnetite Separates for Exploration of Precious Metals in Porphyry-Cu Deposits

Alkaline or K-rich calc-alkaline porphyry deposits worldwide represent significant gold resources, owing to their large sizes. They are derived from hydrous calc-alkaline magmas and are genetically linked to magmatic and hydrothermal processes. Despite their common origin in a supra-subduction environment, platinum-group elements (PGEs) have been recorded only in certain porphyry-Cu deposits. During the last decades, significant Pd and Pt contents were described in the Cordillera of British Columbia, in the Balkan–Karpathian system, including the Skouries deposit, in the Philippines and elsewhere [4,12,13,80,81]. The estimated Pd, Pt, and Au potential for porphyry deposits, combined with the association of merenskyite [(Pd, Pt) $(Te, Bi)_2$)] with major Cu minerals (bornite and chalcopyrite), are considered to be encouraging economic factors for Pd and Pt, as by-products, the Au being the main precious metal product [13,80,81].

It has been suggested that first-stage arc magmas tend to generate Cu-rich, relatively Au-poor porphyry systems, while relatively Au-rich residue is left in the lower crust and lithospheric mantle after first-stage arc magmas [82]. Subsequently, a second stage of melting, due probably to lithospheric thickening, thermal rebound, mantle lithosphere delamination, or lithospheric extension, may generate magmas with relatively high Au/Cu ratios [82–84] and PGE enrichments [84–87]. Critical requirements for a significant base/precious metal potential in porphyry Cu + Au + Pd ± Pt deposits are considered to be the geotectonic environment, controlling the precious/base metal endowment in the parent magma (metasomatized asthenospheric mantle wedge) [86,87]. It is indicated by significant Cr, Co, Ni, and Re contents, the oxidized nature of parent magmas, that facilitate the capacity for transporting sufficient Au and PGE, and the degree of evolution of the mineralized system, as is exemplified by the enrichment of (Pd + Pt) versus (Os + Ir + Ru) and LREE versus HREE [4,86,87]. Arc magmas with high potential to produce hydrothermal systems with ideal chemistry for transporting precious metals (Cu + Au + Pd ± Pt deposits) are characterized by fO_2 more than two log units above fayalite-magnetite-quartz (FMQ), where fO_2 is oxygen fugacity and FMQ is the fayalite–magnetite–quartz oxygen buffer [88]. Since the oxidized nature of parent magma is connected with the ability to produce a magmatic–hydrothermal system with ideal chemistry that facilitates the capacity for transporting sufficient precious metals, abundant magnetite (reaching up to 10 vol.% in the Skouries deposit) linked to pervasive potassic and propylitic alteration type [13], in contrast to "reduced" porphyry Cu–Au deposits, lacking primary hematite, magnetite separates, and sulphate minerals [89], is considered to be a characteristic feature of the Pd-bearing porphyry-Cu deposits. Thus, the abundance of magnetite separates is a characteristic feature of all porphyry-Cu–Au–Pd deposits, as indicated by unexpected high-grade Cu–(Pd + Pt) (up to 6 ppm) mineralization at the Elatsite porphyry deposit, which is found in a spatial association

with the Chelopech epithermal deposit (Bulgaria) and the Skouries porphyry deposit, Greece [4,12]. Disseminated hydrothermal magnetite separate is often associated with fine (less than 10 μm) crystals of U-thorite and zircon within veinlets of quartz (Figure 3c), which is consistent with the elevated Th, U, and Zr contents (Table S1).

The enrichment in Cr, Co ± Ni is a common feature, recorded in the Skouries, Elatsite, and other porphyry deposits of the Balkan Peninsula, characterized by significant Pd and Pt contents, in contrast to the porphyry-Cu ± Mo deposits of Russia and Mongolia with lower (Pd + Pt) content (less than 25 ppm Cr [49,90]) supports the origin of their parent magma from an enriched mantle source [91,92]. In addition, a salient feature is the evolved geochemical signature of the Skouries and Elatsite porphyry-Cu deposits, as indicated by the negative trend between (Pd + Pt) and Cr contents (Figure 14). The application of stable isotope analyses of oxygen ($\delta^{18}O$ = 4.33–9.45‰) and hydrogen (δD = −110‰ to −73‰) on quartz veins from various drill holes and depths may provide evidence to constrain the origin of fluids trapped in quartz veins [85]. Although any systematic variation of the isotopic data with depth is uncertain, it seems likely that the samples with higher Cr contents correspond to lower $\delta^{18}O$ values, while those with lower Cr contents correspond to higher $\delta^{18}O$ values. This isotope variation, coupled with the higher (Pd + Pt) content Pd/Pt ratios corresponding to higher $\delta^{18}O$ values and lower Cr contents, may point toward the more evolved mineralizing system (Figure 14) [86].

6. Conclusions

Texture, mineral chemistry and geochemical data on massive and disseminated magnetite separates from a wide range of geotectonic settings and rock types led us to the following conclusions:

- Magnetite separates of hydrothermal origin associated with calc-alkaline rocks can be distinguished from that associated with ophiolites in terms of their higher Ga content, while magnetite separates of magmatic origin are characterized by the highest (V + Ti) content.
- Hydrothermal magnetite separates from skarn-type (Lavrion mine) differs compared to the disseminated separates from porphyry-Cu deposit (Skouries) in terms of the higher Ba, Bi, Cr, Ni, Co, V, Sr, Sc, Rb, ΣREE, Y, Hf, Th, U, and Zr contents in the latter.
- Although an initial primary magmatic origin for the Fe–Cu–Ni–Co sulphides in the Pindos ophiolite is not precluded, geochemical characteristics (REE-, Ti-, and V-depleted) of the highly transformed magnetite separates may indicate that potential original magmatic features have been overprinted by low-level hydrothermal circulation processes.
- Similarity between the REE patterns, including the clear Eu negative anomaly of magnetite separates from coastal black sand of Kos Island, may provide evidence of an andesitic source.
- A major requirement controlling the Pd and Pt potential of porphyry-Cu deposits is probably the oxidized nature of parent magmas that facilitate the capacity for transporting sufficient Pd and Pt, and the crystallization of abundant magnetite.
- Abundance of magnetite in porphyry-type deposits may be used to discriminate between porphyry-Cu–Au–Pd–Pt and porphyry-Cu–Mo deposits lacking precious metals, providing evidence for the exploration of precious metals in porphyry systems.

Supplementary Materials: The following are available online at http://www.mdpi.com/2075-163X/9/12/759/s1, Table S1: Major and trace element contents in representative magnetite separates from various geotectonic settings (Greece).

Author Contributions: D.G.E. collected the samples, provided the field information, and performed all types of analyses. Both authors (D.G.E. and M.E.-E.) contributed to the elaboration and interpretation of the data. The writing of the paper was completed by M.E.-E.

Funding: This research was funded by the National and Kapodistrian University of Athens (NKUA) (Grant No. KE_11730).

Acknowledgments: Many thanks are expressed to the two anonymous reviewers for their constructive criticism and suggestions on an earlier draft of the manuscript. Vassilis Skounakis, University of Athens, is thanked for his assistance with the SEM/EDS analyses.

Conflicts of Interest: The authors declare no conflicts of interest.

References

1. Paraskevopoulos, G.M.; Economou, M.I. Zoned Mn-rich chromite from podiform type chromite ore in serpentinites of northern Greece. *Am. Miner.* **1981**, *66*, 1013–1019.
2. Economou, M.; Skounakis, S.; Papathanasiou, C. Magnetite deposits of skarn type from the Plaka area of Laurium. *Greece* **1981**, *40*, 241–252.
3. Lindsley, D.H. Experimental studies of oxide minerals: Reviews Mineral. *Geochemistry* **1991**, *25*, 69–106.
4. Eliopoulos, D.G.; Economou-Eliopoulos, M. Platinum-group element and gold contents in the Skouries porphyry-copper deposit, Chalkidiki Peninsula, northern Greece. *Econ. Geol.* **1991**, *86*, 740–749. [CrossRef]
5. Dupuis, C.; Beaudoin, G. Discriminant diagrams for iron oxide trace element fingerprinting of mineral deposit types. *Miner. Depos.* **2011**, *46*, 319–335. [CrossRef]
6. Dare, S.A.S.; Barnes, S.-J.; Beaudoin, G. Variation in trace element content of magnetite crystallized from a fractionating sulfide liquid, Sudbury, Canada: Implications for provenance discrimination. *Geochim. Cosmoch. Acta* **2012**, *88*, 27–50. [CrossRef]
7. Nadoll, P.; Mauk, J.L.; Hayes, T.S.; Koenig, A.E.; Box, S.E. Geochemistry of magnetite from hydrothermal ore deposits and host rocks of the Mesoproterozoic Belt Supergroup, United States. *Econ. Geol.* **2012**, *107*, 1275–1292. [CrossRef]
8. Nadoll, P.; Angerer, T.; Mauk, J.L.; French, D.; Walshe, J. The chemistry of hydrothermal magnetite: A review. *Ore. Geol. Rev.* **2014**, *61*, 1–32. [CrossRef]
9. Dare, S.A.; Barnes, S.-J.; Beaudoin, G.; Mıric, J.; Boutroy, E.; Potvin-Doucet, C. Trace elements in magnetite as petrogenetic indicators. *Miner. Depos.* **2012**, *49*, 785–796. [CrossRef]
10. Rapp, J.F.; Klemme, S.; Butler, I.B.; Harley, S.L. Extremely high solubility of rutile in chloride and fluoride-bearing metamorphic fluids: An experimental investigation. *Geology* **2010**, *38*, 323–326. [CrossRef]
11. Economou-Eliopoulos, M. Apatite and Mn, Zn, Co-enriched chromite in Ni-laterites of northern Greece and their genetic significance. *J. Geochem. Exp.* **2003**, *80*, 41–54. [CrossRef]
12. Augé, T.; Petrunov, R.; Bailly, L. On the mineralization of the PGE mineralization in the Elastite porphyry Cu–Au deposit, Bulgaria: Comparison with the Baula-Nuasahi Complex, India, and other alkaline PGE-rich porphyries. *Can. Miner.* **2005**, *43*, 1355–1372. [CrossRef]
13. Economou-Eliopoulos, M. Platinum-Group Element Potential of Porphyry Deposits. In *Mineralogical Association of Canada Short Course 35*; Mineralogical Association of Canada: Quebec, QC, Canada, 2005; pp. 203–245.
14. Navrotsky, A.; Kleppa, O.J. The thermodynamics of cation distributions in simple spinels. *J. Inorg. Nucl. Chem.* **1967**, *29*, 2701–2714. [CrossRef]
15. O'Neill, H.C.; Navrotsky, A. Simple spinels: Crystallographic parameters, cation radii, lattice energies, and cation distribution. *Am. Miner.* **1983**, *68*, 181–194.
16. Hu, H.; Lentz, D.; Li, J.W.; McCarron, T.; Zhao, X.F.; Hall, D. Reequilibration processes in magnetite from iron skarn deposits. *Econ. Geol.* **2015**, *110*, 1–8. [CrossRef]
17. Marinos, G.P.; Petrascheck, W.E. Laurium. *Geol. Geophys. Res.* **1956**, *4*, 1–247.
18. Skarpelis, N.; Tsikouris, B.; Pe-Piper, G. The Miocene igneous rocks in the Basal Unit of Lavrion (SE Attica, Greece): Petrology and geodynamic implications. *Geol. Mag.* **2007**, *145*, 1–15. [CrossRef]
19. Voudouris, P.; Melfos, V.; Spry, P.; Bonsall, T.; Tarkian, M.; Economou-Eliopoulos, M. Mineralogical and fluid inclusion constraints on the evolution of the Plaka intrusion-related ore system, Lavrion, Greece. *Miner. Petrol.* **2008**, *93*, 79–110. [CrossRef]
20. Ducoux, M.; Branquet, Y.; Jolivet, L.; Arbaret, L.; Grasemann, B.; Rabillard, A.; Gumiaux, C.; Drufin, S. Synkinematic skarns and fluid drainage along detachments: The West Cycladic Detachment System on Serifos Island (Cyclades, Greece) and its related mineralization. *Tectonophysics* **2017**, *695*, 1–26. [CrossRef]
21. Kockel, F.; Mollat, H.; Gundlach, H. Hydrothermally altered and (copper) mineralizedp orphyritic intrusionsin the ServomacedoniaMn assif s (Greece). *Miner. Depos.* **1975**, *10*, 195–204. [CrossRef]

22. Pearce, J.A.; Lippard, S.J.; Roberts, S. Characteristics and tectonic significance of supra-subduction zone ophiolites. *Geol. Soc. Lond. Spec. Pub.* **1984**, *16*, 77–94. [CrossRef]
23. Saccani, E.; Photiades, A.; Santato, A.; Zeda, O. New evidence for supra-subduction zone ophiolites in the Vardar Zone from the Vermion Massif (northern Greece): Implication for the tectono-magmatic evolution of the Vardar oceanic basin. *Ofioliti* **2008**, *33*, 17–37.
24. Economou-Eliopoulos, M.; Eliopoulos, D.; Chryssoulis, S. A comparison of high-Au massive sulfide ores hosted in ophiolite complexes of the Balkan Peninsula with modern analogues: Genetic significance. *Ore Geol. Rev.* **2008**, *33*, 81–100. [CrossRef]
25. Paraskevopoulos, G.M.; Economou, M.I. Genesis of magnetite ore occurrences by metasomatism of chromite ores in Greece. *Neues Jahrb. Fur Miner. Abh.* **1980**, *140*, 29–53.
26. Mercier, J. Édute géologique des zones internes des Hellénides en Macédoine centrale (Grèce). Ire Thèse (1966). *Ann. Géol. Des. Pays Hell.* **1968**, *20*, 596.
27. Sideris, C.; Skounakis, S.; Economou, M. The ophiolite complex of Edessa area and the associated mineralization. International Symposium on metallogeny of mafic and ultramafic complexes. *I.G.C.P. 169 Athens* **1980**, *2*, 142–153.
28. Hynes, A.J. The Geology of Part of the Western Othrys Mountains, Greece. Ph.D. Thesis, University of Cambridge, Cambridge, UK, 1972.
29. Rassios, A.; Dilek, Y. Rotational deformation in the Jurassic Mesohellenic Ophiolites, Greece, and its tectonic significance. *Lithos* **2009**, *108*, 207–223. [CrossRef]
30. Rassios, A.; Konstantopoulou, G. Emplacement tectonism and the position of chrome ores in the Mega Isoma peridotites, SW Othris, Greece. *Bull. Geol. Soc. Greece* **1993**, *28*, 463–474.
31. Mitsis, I.; Economou-Eliopoulos, M. Occurrence of apatite with magnetite in an ophiolite complex (Othrys), Greece. *Am. Miner.* **2001**, *86*, 1143–1150. [CrossRef]
32. Paraskevopoulos, G.; Economou, M. Komatiite-type ultramafic lavas from the Agrilia Formation, Othrys ophiolite complex, Greece. *Ofioliti* **1986**, *11*, 293–304.
33. Economou-Eliopoulos, M.; Paraskevopoulos, G. Platinum -group elements and gold in komatiitic rocks from the Agrilia Formation, Othrys ophiolite complex, Greece. *Chem. Geol.* **1989**, *77*, 149–158. [CrossRef]
34. Koutsovitis, P.; Magganas, A.; Ntaflos, T. Rift and intra-oceanic subduction signatures in the Western Tethys during the Triassic: The case of ultramafic lavas as part of an unusual ultramafic–mafic–felsic suite in Othris, Greece. *Lithos* **2012**, *144*, 177–193. [CrossRef]
35. Baziotis, I.; Economou-Eliopoulos, M.; Asimow, P.D. Ultramafic lavas and high-Mg basaltic dykes from the Othris ophiolite complex, Greece. *Lithos* **2017**, *288*, 231–247. [CrossRef]
36. Rassios, A. Geology and Evolution of the Vourinos Complex, Northern Greece. Ph.D. Thesis, University of California (Davis), Davis, CA, USA, 1981.
37. Francalanci, L.; Varekamp, J.C.; Vougioukalakis, G.; Defant, M.J.; Innocenti, F.; Manetti, P. Crystal retention, fractionation and crustal assimilation in aconvecting magma chamber Nisyros Volcano, Greece. *Bull. Volcanol.* **1995**, *56*, 601–620. [CrossRef]
38. Papanikolaou, D. Geotectonic evolution of the Aegean. *Bull. Geol. Soc. Greece* **1993**, *27*, 33–48.
39. Royden, L.H.; Papanikolaou, D.J. Slab segmentation and late Cenozoicdisruption of the Hellenic arc. *Geochem. Geophys. Geosyst.* **2011**, *12*, Q03010. [CrossRef]
40. Mitropoulos, P.; Tarney, J.; Saunders, A.D.; Marsh, N.G. Petrogenesis of Cenozoic rocks from the aegean island arc. *J. Volcanol. Geotherm. Res.* **1987**, *32*, 177–193. [CrossRef]
41. Tzifas, I.T.; Misaelides, P.; Godelitsas, A.; Gamaletsos, P.N.; Nomikou, P.; Karydas, A.G.; Kantarelou, V.; Papadopoulos, A. Geochemistry of coastal sands of Eastern Mediterranean: The case of Nisyros volcanic materials. *Chem. Der Erde-Geochem.* **2017**, *77*, 487–501. [CrossRef]
42. Marcopoulos, T.; Economou, M. Theophrastite, $Ni(OH)_2$, a new mineral from Northern Greece. *Am. Miner.* **1981**, *66*, 1020–1021.
43. Economou-Eliopoulos, M.; Eliopoulos, D. *A New Solid Solution [(Co,Mn,Nn)(OH)$_2$], in the Vermion Mt (Greece) and its Genetic Significance for the Mineral Group of Hydroxides*; McLaughlin, E.D., Braux, L.A., Eds.; Chemical Mineralogy, Smelting and Metallization; Nova Science Publishers: New York, NY, USA, 2009; pp. 1–18.
44. Taylor, S.R.; McLennan, S.M. *The Continental Crust: Its Composition and Evolution*; Blackwell Scientific: Oxford, UK, 1985.

45. Gamaletsos, P. Mineralogy and Geochemistry of Bauxites from Parnassos-Ghiona Mines and the Impact on the Origin of the Deposits. Ph.D. Thesis, University of Athens, Athens, Greece, 2014.
46. Kalatha, S. Metallogenesis of Bauxite Laterites and Fe-Ni-laterites-Enrichnment in Rare Earth Elements. Ph.D. Thesis, University of Athens, Athens, Greece, 2017.
47. Barth, M.; Gluhak, T. Geochemistry and tectonic setting of mafic rocks from the Othris Ophiolite, Greece. *Contrib. Miner. Petrol.* **2009**, *157*, 23–40. [CrossRef]
48. McDonough, W.F.; Sun, S.S. Chemical evolution of the mantle. The composition of the Earth. *Chem. Geol.* **1995**, *120*, 223–253. [CrossRef]
49. Sotnikov, V.I.; Berzina, A.N.; Economou-Eliopoulos, M.; Eliopoulos, D.G. Palladium, platinum and gold distribution in porphyry Cu _ Mo deposits of Russia and Mongolia. *Ore Geol. Rev.* **2001**, *18*, 95–111. [CrossRef]
50. Schock, H.H. Distribution of rare-earth and other trace elements in magnetite separates. *Chem. Geol.* **1979**, *26*, 119–133. [CrossRef]
51. Deditius, A.P.; Reich, M.; Simon, A.C.; Suvorova, A.; Knipping, J.; Roberts, M.P.; Rubanov, S.; Dodd, A.; Saunders, M. Nanogeochemistry of hydrothermal magnetite. *Contrib. Miner. Petrol.* **2018**, *173*, 46. [CrossRef]
52. Horn, I.; Foley, S.F.; Jackson, S.E.; Jenner, G.A. Experimental determined partitioning of high field strength and selected transition elements between spinel and basaltic melt. *Chem. Geol.* **1994**, *117*, 193–318. [CrossRef]
53. Balaram, V. Rare earth elements: A review of applications, occurrence, exploration, analysis, recycling, and environmental impact. *Geosci. Front.* **2019**, *10*, 1285–1303. [CrossRef]
54. Maksimovic, Z.; Skarpelis, N.; Panto, G. Mineralogy and geochemistry of the rare earth elements in the karstic nickel deposit of Lokris area, Greece. *Acta Geol. Hung.* **1993**, *36*, 331–342.
55. Economou-Eliopoulos, M.; Eliopoulos, D.G.; Apostolikas, A.; Maglaras, K. Precious and rare earth element distribution in Ni-laterite deposits from Lokris area, Central Greece. In Proceedings of the Fourth Biennial SGA Meeting, Turku, Finland, 11–13 August 1997; pp. 411–413.
56. Kalatha, S.; Perraki, M.; Economou-Eliopoulos, M.; Mitsis, I. On the origin of bastnaesite-(La,Nd,Y) in the Nissi (Patitira) bauxite laterite deposit, Lokris, Greece. *Minerals* **2017**, *7*, 45. [CrossRef]
57. Goodenough, K.M.; Schilling, J.; Jonsson, E.; Kalvig, P.; Charles, N.; Tuduri, J.; Deady, E.A.; Sadeghi, M.; Schiellerup, H.; Muller, A.; et al. Europe's rare earth element resource potential: An overview of REE metallogenetic provinces and their geodynamic setting. *Ore Geol. Rev.* **2016**, *72*, 838–856. [CrossRef]
58. Colony, W.E.; Nordlie, B.E. Liquid sulfur at Volcan Azufre, Galapagos Islands. *Econ. Geol.* **1973**, *68*, 371–380. [CrossRef]
59. GustafsonL, B.; Hunt, J.P. The porphyry copper deposit at E1 Salvador, Chile. *Econ. Geol.* **1975**, *70*, 857–912. [CrossRef]
60. Hemley, J.J.; Hunt, J.P. Hydrothermal ore-forming processes in the light of studies in rock-buffered systems. II. Some general geologic applications. *Econ. Geol.* **1992**, *87*, 23–43.
61. Hemley, J.J.; Cygan, G.L.; Fein, J.B.; Robinson, G.R.; d'Angelo, W.M. Hydrothermal ore-forming processes in the light of studies in rock-buffered systems I.: Iron-copper-zinc-lead sulfide solubility relations. *Econ. Geol.* **1992**, *87*, 1–22. [CrossRef]
62. Bliss, N.W.; MacLean, W.H. The paragenesis of zoned chromite from central Manitoba. *Geochim. Cosmochim. Acta* **1975**, *39*, 973–990. [CrossRef]
63. Bosi, F.; Andreozzi, G.B.; Hålenius, U.; Skogby, H. Zn-O tetrahedral bond length variations in normal spinel oxides. *Am. Mineral.* **2011**, *96*, 594–598. [CrossRef]
64. Martignago, F.; Dal Negro, A.; Carbonin, S. How Cr^{3+} and Fe^{3+} affect Mg-Al order disorder transformation at high temperature in natural spinels. *Phys. Chem. Miner.* **2003**, *30*, 401–408. [CrossRef]
65. Gervilla, F.; Padrón-Navarta, J.A.; Kerestedjian, T.; Sergeeva, I.; González-Jiménez, J.M.; Fanlo, I. Formation of ferrian chromite in podiform chromitites from the Golyamo Kamenyane serpentinte, Eastern Rhodopes,SE Bulgaria: A two-stage process. *Contrib. Mineral. Petrol.* **2012**, *164*, 643–657. [CrossRef]
66. Colás, V.; González-Jiménez, J.M.; Griffin, W.L.; Fanlo, I.; Gervilla, F.; O'Reilly, S.Y.; Pearson, N.J.; Kerestedjian, T.; Proenza, J.A. Fingerprints of metamorphism in chromite: New insights from minor and trace elements. *Chem. Geol.* **2014**, *389*, 137–152. [CrossRef]
67. Glemser, O.; Einerhand, J. Uber hohere Nickelhydroxide. *Z. Anorg. Chem.* **1950**, *261*, 26–42. [CrossRef]
68. Baskar, S.; Baskar, R.; Kaushik, A. Role of microorganisms in weathering of the Konkan-Goa laterite formation. *Curr. Sci.* **2003**, *85*, 1129–1134.

69. Russell, M.J.; Hall, A.J.; Boyce, A.J.; Fallick, A.E. On hydrothermal convection systems and the emergence of life. *Econ. Geol.* **2005**, *100*, 418–438.
70. Southam, G.; Saunders, J. The geomicrobiology of ore deposits. *Econ. Geol.* **2005**, *100*, 1067–1084. [CrossRef]
71. Valeton, I.; Biermann, M.; Reche, R.; Rosenberg, F. Genesis of Nickel laterites and bauxites in Greece during the Jurassic and Cretaceous, and their relation to ultrabasic parent rocks. *Ore Geol. Rev.* **1987**, *2*, 359–404. [CrossRef]
72. Eliopoulos, D.; Economou-Eliopoulos, M. Geochemical and mineralogical characteristics of Fe–Ni and bauxite–laterite deposits of Greece. *Ore Geol. Rev.* **2000**, *16*, 41–58. [CrossRef]
73. Kalatha, S.; Economou-Eliopoulos, M. Framboidal pyrite and bacteriomorphic goethite at transitional zones between Fe–Ni–laterites and limestones: Evidence from Lokris, Greece. *Ore Geol. Rev.* **2015**, *65*, 413–425. [CrossRef]
74. Norton, S. Laterite and bauxite formation. *Econ. Geol.* **1973**, *63*, 353–361. [CrossRef]
75. Laskou, M.; Economou-Eliopoulos, M. The role of microorganisms on the mineralogical and geochemical characteristics of the Parnassos-Ghiona bauxite deposits, Greece. *J. Geochem. Explor.* **2007**, *93*, 67–77. [CrossRef]
76. Laskou, M.; Economou-Eliopoulos, M. Bio-mineralization and potential biogeochemical processes in bauxite deposits: Genetic and ore quality significance. *Miner. Petrol.* **2013**, *107*, 471–486. [CrossRef]
77. Schulte, R.F.; Foley, N.K. *Compilation of Gallium Resource Data for Bauxite Deposits*; U.S. Geological Survey: Reston, VA, USA, 2014.
78. Zhou, M.F.; Robinson, P.T.; Su, B.X.; Gao, J.F.; Li, J.W.; Yang, J.S.; Malpas, J. Compositions of chromite, associated minerals, and parental magmas of podiform chromite deposits: The role of slab contamination of asthenospheric melts in suprasubduction zone environments. *Gondwana Res.* **2014**, *26*, 262–283. [CrossRef]
79. Eliopoulos, I.P.D.; Eliopoulos, G.D. Factors Controlling the Gallium Preference in High-Al Chromitites. *Minerals* **2019**, *9*, 623. [CrossRef]
80. Tarkian, M.; Koopmann, G. Platinum-group minerals in the Santo Tomas II (Philex) porphyry copper–gold deposit, Luzon Island, Philippines. *Miner. Depos.* **1995**, *30*, 39–47. [CrossRef]
81. Thompson, J.F.H.; Lang, J.R.; Stanley, C.R. Platinum-group elements in alkaline porphyry deposits, British Columbia. *Explor. Min. B. C. Mines Branch Part B* **2001**, *2001*, 57–64.
82. Richards, J.P. Tectono-magmatic precursors for porphyry Cu–(Mo–Au) deposit formation. *Econ. Geol.* **2003**, *98*, 1515–1533. [CrossRef]
83. Richards, J.P. Postsubduction porphyry Cu–Au and epithermal Au deposits: Products of remelting of subduction-modified lithosphere. *Geology* **2009**, *37*, 247–250. [CrossRef]
84. Richards, J. Tectonic, magmatic, metallogenic evolution of the Tethyan orogeny: From subduction to collision. *Ore Geol. Rev.* **2015**, *70*, 323–345. [CrossRef]
85. Tarkian, M.; Hünken, U.; Tokmakchieva, M.; Bogdanov, K. Precious-metal distribution and fluid-inclusion petrography of the Elatsite porphyry copper deposit, Bulgaria. *Miner. Depos.* **2003**, *38*, 261–281. [CrossRef]
86. Eliopoulos, D.G.; Economou-Eliopoulos, M.; Zelyaskova-Panayiotova, M. Critical factors controlling Pd and Pt potential in porphyry Cu–Au deposits: Evidence from the Balkan Peninsula. *Geosciences* **2014**, *4*, 31–49. [CrossRef]
87. Holwell, D.; Fiorentini, M.; McDonald, I.; Lu, Y.; Giuliani, A.; Smith, D.; Keith, M.; Locmelis, M. A metasomatized lithospheric mantle control on the metallogenic signature of post-subduction magmatism. *Nat. Commun.* **2019**, *10*, 1–10. [CrossRef]
88. Mungall, J.E.; Andrews, D.R.A.; Cabri, L.J.; Sylvester, P.J.; Tubrett, M. Partitioning of Cu, Ni, Au, and platinum-group elements between monosulfide solid solution and sulfide melt under controlled oxygen and sulphur fugacities. *Geochim. Cosmochim. Acta* **2005**, *69*, 4349–4360. [CrossRef]
89. Sillitoe, R.H. Porphyry copper systems. *Econ. Geol.* **2010**, *105*, 3–41. [CrossRef]
90. Berzina, A.P.; Berzina, A.N.; Gimon, V.O. Paleozoic–Mesozoic porphyry Cu (Mo) and Mo (Cu) deposits within the southern margin of the Siberian Craton: Geochemistry, geochronology, and petrogenesis (a review). *Minerals* **2016**, *6*, 125. [CrossRef]

91. McInnes, B.I.A.; Cameron, E.M. Carbonated, alkaline hybridizing melts from a sub-arc environment: Mantle wedge samples from the Tabar-Lihir-Tanga-Feni arc, Papua New Guinea. *Earth Planet. Sci. Lett.* **1994**, *122*, 125–141. [CrossRef]
92. Moritz, R.; Kouzmanov, K.; Petrunov, R. Upper Cretaceous Cu–Au epithermal deposits of the Panagyurishte district, Srednogorie zone, Bulgaria. *Swiss Bull. Miner. Petrol.* **2004**, *84*, 79–99.